



**fire**  
cci

---


## **ESA Climate Change Initiative – Fire\_cci**

### **D2.1.1 Algorithm Theoretical Basis Document (ATBD) – MERIS**

---

|                      |  |
|----------------------|--|
| <b>Project Name</b>  | ECV Fire Disturbance: Fire_cci Phase 2                           |
| <b>Contract Nº</b>   | 4000115006/15/I-NB   |
| <b>Issue Date</b>    | 11/11/2016   |
| <b>Version</b>       | 1.1  |
| <b>Author</b>        | Itziar Alonso-Canas, Emilio Chuvieco, Grit Kirches, Thomas Storm |
| <b>Document Ref.</b> | Fire_cci_D2.1.1_YR1_ATBD-MERIS_v1.1                              |
| <b>Document type</b> | Public   |

*To be cited as: Alonso-Canas I, Chuvieco E., Kirches G., Storm T. (2016) ESA CCI ECV Fire Disturbance: Algorithm Theoretical Basis Document-MERIS, version 1.1. Available at: <http://www.esa-fire-cci.org/documents>*

|   |  |   |                 |  |
|---|--|---|-----------------|--|
|  | <b>Fire_cci</b><br><b>Algorithm Theoretical Basis</b><br><b>Document – MERIS</b> | Ref.: Fire_cci_D2.1.1_YR1_ATBD-MERIS_v1.1 |                 |  |
|   |  | Issue 1.1                                 | Date 11/11/2016 |  |
|   |  |   | Page 2          |  |


## Project Partners

|  |   |
|--|---|
| Prime Contractor/<br>Scientific Lead & Project<br>Management | UAH – University of Alcalá (Spain)                            |
| Earth Observation Team                                       | UAH – University of Alcalá (Spain)                            |
|  | EHU – University of the Basque Country (Spain)                |
|  | UL – University of Leicester (United Kingdom)                 |
|  | UCL – University College London (United Kingdom)              |
|  | ISA – School of Agriculture, University of Lisbon (Portugal)  |
| System Engineering   | BC – Brockmann Consult GmbH (Germany)                         |
| Climate Research Group                                       | MPIC – Max Planck Institute for Chemistry (Germany)           |
|  | IRD - Research Institute for Development (France)             |
|  | LSCE - Climate and Environmental Sciences Laboratory (France) |
|  | VUA - Stichting VU-VUmc (Netherlands)                         |



## Distribution

| Affiliation              | Name                         | Address                               | Copies          |
|--------------------------|------------------------------|---------------------------------------|-----------------|
| ESA                      | Stephen Plummer (ESA)        | stephen.plummer@esa.int               | electronic copy |
| Project Team             | Emilio Chuvieco, (UAH)       | emilio.chuvieco@uah.es                | electronic copy |
|                          | M. Lucrecia Pettinari (UAH)  | mlucrecia.pettinari@uah.es            |                 |
|                          | Itziar Alonso (UAH)          | itziar.alonsoc@uah.es                 |                 |
|                          | Aitor Bastarrika (EHU)       | aitor.bastarrika@ehu.es               |                 |
|                          | Ekhi Roteta (EHU)            | ekhi.roteta@gmail.com                 |                 |
|                          | Kevin Tansey (UL)            | kjt7@leicester.ac.uk                  |                 |
|                          | Marc Padilla Parellada (UL)  | mp489@leicester.ac.uk                 |                 |
|                          | James Wheeler (UL)           | jemw3@leicester.ac.uk                 |                 |
|                          | Philip Lewis (UCL)           | ucfalew@ucl.ac.uk                     |                 |
|                          | José Gómez Dans (UCL)        | j.gomez-dans@ucl.ac.uk                |                 |
|                          | James Brennan (UCL)          | james.brennan.11@ucl.ac.uk            |                 |
|                          | Jose Miguel Pereira (ISA)    | jmocpereira@gmail.com                 |                 |
|                          | Duarte Oom (ISA)             | duarte.oom@gmail.com                  |                 |
|                          | Manuel Campagnolo (ISA)      | mlc@isa.ulisboa.pt                    |                 |
|                          | Thomas Storm (BC)            | thomas.storm@brockmann-consult.de     |                 |
|                          | Martin Böttcher (BC)         | martin.boettcher@brockmann-consult.de |                 |
|                          | Grit Kirches (BC)            | grit.kirches@brockmann-consult.de     |                 |
|                          | Johannes Kaiser (MPIC)       | j.kaiser@mpic.de                      |                 |
|                          | Angelika Heil (MPIC)         | a.heil@mpic.de                        |                 |
|                          | Florent Mouillot (IRD)       | florent.mouillot@cefe.cnrs.fr         |                 |
|                          | Philippe Ciais (LSCE)        | philippe.ciais@lsce.ipsl.fr           |                 |
| Patricia Cadule (LSCE)   | patricia.cadule@lsce.ipsl.fr |                                       |                 |
| Chao Yue (LSCE)          | chaoyuejoy@gmail.com         |                                       |                 |
| Guido van der Werf (VUA) | guido.vander.werf@vu.nl      |                                       |                 |

|   |  |  |   |                 |
|---|--|--|---|-----------------|
|  | <b>Fire_cci</b><br><b>Algorithm Theoretical Basis</b><br><b>Document – MERIS</b> |  | Ref.: Fire_cci_D2.1.1_YR1_ATBD-MERIS_v1.1 |                 |
|   |  |  | Issue 1.1                                 | Date 11/11/2016 |
|   |  |  | Page 3                                    |                 |

## Summary

This document presents the technical basis of the algorithms used to generate the Fire\_cci Burned Area product v4.1, based on MERIS full resolution data. The document analyses the input requirements and the process to create the product.

|                   | Affiliation/Function                    | Name   | Date       | Signature |
|-------------------|---|--|------------|-----------|
| <b>Prepared</b>   | UAH<br>UAH - Science Leader<br>BC<br>BC | Itziar Alonso-Canas<br>Emilio Chuvieco<br>Grit Kirches<br>Thomas Storm | 10/11/2016 |           |
| <b>Reviewed</b>   | UAH – Project Manager                   | Lucrecia Pettinari   | 10/11/2016 |           |
| <b>Authorized</b> | UAH - Science Leader                    | Emilio Chuvieco  | 11/11/2016 |           |
| <b>Accepted</b>   | ESA - Technical Officer                 | Stephen Plummer  | 14/12/2016 |           |

This document is not signed. It is provided as an electronic copy.

## Document Status Sheet

| Issue      | Date       | Details   |
|------------|------------|---|
| <b>1.0</b> | 02/08/2016 | First issue of the document.                                      |
| <b>1.1</b> | 11/11/2016 | Addressing ESA comments according to CCI_FIRE_EOPS_MM_16_0102.pdf |
|            |            |   |

## Document Change Record

| Issue    | Date                | Request | Location  | Details   |
|----------|---------------------|---------|---|---|
| 1.1      | 11/11/2016          | ESA     | Naming convention   | Reference to the year of the project added to the name of the document.                                       |
|          |                     |         | Section 1.1   | Purpose of the document clarified and expanded.   |
|          |                     |         | Section 3.1   | Revised and updated.  |
|          |                     |         | Sections 2.2, 3.2.1, 3.3, 3.3.2.1, 3.3.2.3, 3.3.3.5, 3.3.5.2, 3.3.5, 4.1, 4.3 | Minor changes in the text.  |
|          |                     |         | Section 3.1   | Minor changes in the text, and Figure 1 updated.  |
|          |                     |         | Section 3.1.1   | Updated.  |
|          |                     |         | Section 3.2.2   | Clarification regarding the length of the MERIS time series considered, and the meaning of segregated images. |
|          |                     |         | Section 3.3.2.3   | Last paragraph updated.   |
|          |                     |         | Section 3.3.3   | Minor changes and footnote added.   |
|          |                     |         | Section 3.3.3.1   | Information and footnote added.   |
|          |                     |         | Section 3.3.3.2   | Updated information.  |
|          |                     |         | Section 3.3.4   | Clarification of the sources of the methods used.   |
|          |                     |         | References  | Some references have been deleted and others added.   |
| Acronyms | New acronyms added. |         |   |   |



## **Table of Contents**

|   |           |
|---|-----------|
| <b>1. Executive Summary .....</b>   | <b>7</b>  |
| 1.1. Purpose of the document .....  | 7         |
| 1.2. Applicable Documents.....  | 7         |
| 1.3. Applicable Documents.....  | 7         |
| 1.4. Document Structure .....   | 7         |
| <b>2. Introduction .....</b>  | <b>8</b>  |
| 2.1. Background.....  | 8         |
| 2.2. Purpose of the document .....  | 8         |
| <b>3. Pre-processing Chain .....</b>  | <b>9</b>  |
| 3.1. General overview .....   | 9         |
| 3.2. Quality Control of the input products .....  | 10        |
| 3.2.1. Methods.....   | 10        |
| 3.2.2. Results .....  | 10        |
| 3.3. Fire_cci pre-processing chain .....  | 11        |
| 3.3.1. Geometric correction.....  | 11        |
| 3.3.2. Radiometric Calibration .....  | 11        |
| 3.3.2.1. MERIS calibration.....   | 11        |
| 3.3.2.2. Coherent noise equalisation.....   | 11        |
| 3.3.2.3. Smile correction.....  | 12        |
| 3.3.3. Land water delineation and cloud screening - pixel identification .....                  | 12        |
| 3.3.3.1. Pixel identification.....  | 13        |
| 3.3.3.2. Practical consideration.....   | 13        |
| 3.3.3.3. Adaptation of IdePix.....  | 18        |
| 3.3.3.4. Error budget estimates .....   | 19        |
| 3.3.3.5. Cloud shadow and cloud edge detection .....  | 19        |
| 3.3.4. Atmospheric correction - aerosol and spectral directional reflectance<br>retrieval ..... | 21        |
| 3.3.5. Clear land filtering .....   | 24        |
| 3.3.5.1. Clear land feature of IdePix.....  | 24        |
| 3.3.5.2. Temporal filtering.....  | 25        |
| 3.3.6. Temporal sample aggregation .....  | 26        |
| 3.3.7. L3-Processing .....  | 27        |
| 3.3.7.1. Plate-Carrée projection .....  | 27        |
| 3.3.7.2. Resampling .....   | 28        |
| 3.3.7.3. Generation of mosaics .....  | 28        |
| <b>4. BA Algorithm description.....</b>   | <b>29</b> |
| 4.1. General scheme.....  | 29        |



|   |           |
|---|-----------|
| 4.2. Input data .....                                 | 30        |
| 4.3. Bands and indices selection .....                | 31        |
| 4.4. Monthly and annual composites .....              | 32        |
| 4.5. Seed phase .....                                 | 35        |
| 4.5.1. Threshold selection .....                      | 37        |
| 4.5.2. Seed identification.....                       | 37        |
| 4.6. Growing phase .....                              | 38        |
| 4.7. MERIS BA algorithm auxiliary output layers ..... | 40        |
| <b>5. Formatting tool .....</b>                       | <b>41</b> |
| 5.1. Pixel product.....                               | 41        |
| 5.1.1. JD .....                                       | 41        |
| 5.1.2. CL.....  | 41        |
| 5.1.3. LC.....  | 42        |
| 5.2. Grid product.....                                | 42        |
| 5.2.1. Sum of BA (burned_area) .....                  | 42        |
| 5.2.2. Standard error (SE).....                       | 43        |
| 5.2.3. Fraction of observed area (OAF) .....          | 43        |
| 5.2.4. Number of patches (patch_number).....          | 43        |
| 5.2.5. Sum of BA of each LC class .....               | 44        |
| 5.3. Product availability .....                       | 44        |
| <b>6. References .....</b>                            | <b>45</b> |
| <b>Annex 1: Acronyms and abbreviations .....</b>      | <b>49</b> |

**List of Tables**

|   |    |
|---|----|
| Table 1 Results of the QA of MERIS FRS (L1b) from 2003-2012 ..... | 10 |
| Table 2: Feature - Pixel identification .....                     | 13 |
| Table 3: Feature Definition for MERIS.....                        | 14 |
| Table 4: Processing logic.....                                    | 16 |
| Table 5: Thresholds .....   | 17 |
| Table 6: Final status flag .....                                  | 26 |
| Table 7: Variables used in Level 3 mosaicking for MERIS.....      | 28 |

**List of Figures**

|   |    |
|---|----|
| Figure 1: Schematic representation of the Fire_cci pre-processing chain including input (pre-processing chain based on the GlobAlbedo and Land Cover CCI chain) ..... | 9  |
| Figure 2: Original MERIS FRS L1b coastline - green, SRTM SWBD Land/water map - brown.....   | 18 |
| Figure 3: Cloud, cloud edges and cloud shadow .....   | 20 |



Figure 4: Breadboard cloud shadow algorithm - here shown on a Landsat image a) blue channel with cloud shadow potential area border for the biggest cloud yellow) b) k-means cluster analysis result for this cloud c) blue channel with cloud shadow for this cloud d) SWIR channel with cloud shadow for both clouds ..... 21

Figure 5: Algorithm main scheme definition. .... 30

Figure 6: Temporal evolution of NIR and GEMI for a pixel in Portugal..... 32

Figure 7: Temporal evolution of NIR and GEMI for a pixel in Portugal..... 32

Figure 8: HS Thiessen matrix for Northern Australia in October 2008. .... 33

Figure 9: Monthly composites generation based on MERIS information from two consecutive months. .... 34

Figure 10: NIR post fire and julian dates composites for Australia in October 2008. ... 34

Figure 11: Maximum annual GEMI, October 2008 GEMI and difference between them in Australia. .... 35


Figure 12: Steps to build the final composites. .... 35

Figure 13: Normal distributions and CDFs showing the poor and better separation between classes..... 36

Figure 14: Selection of PAF within a MERIS 3x3 window with a HS. .... 37

Figure 15: Main steps to identify seed pixels. .... 38

Figure 16: Growing phase main steps. .... 39

|   |                                    |  |   |     |      |            |
|---|------------------------------------|--|---|-----|------|------------|
|  | <b>Fire_cci</b>                    |  | Ref.: Fire_cci_D2.1.1_YR1_ATBD-MERIS_v1.1 |     |      |            |
|   | <b>Algorithm Theoretical Basis</b> |  | Issue                                     | 1.1 | Date | 11/11/2016 |
|   | <b>Document – MERIS</b>            |  |   |     | Page | 7          |

## 1. Executive Summary

### 1.1. Purpose of the document

Following the Statement of Work of Fire\_cci phase 2 [AD-3 and 4], the first global processing cycle was based on MERIS full resolution data (FRS), following the experience of the Fire\_cci consortium in phase 1 of the programme. This document presents the technical basis of the algorithms used to generate this Fire\_cci Burned Area product, which has been identified as v4.1. This product is currently available in the CCI Data portal and covers the period from 2005 to 2011. The document analyses the algorithms used to create the BA product, including the pre-processing steps performed (e.g. geometric and radiometric corrections to generate corrected reflectances), the stages of the processor to get the burned area data, and the formatting of the data to obtain the released product.

### 1.2. Applicable Documents

### 1.3. Applicable Documents

|        |   |
|--------|---|
| [AD-1] | ESA Climate Change Initiative - CCI Project Guidelines. Ref. EOP-DTEX-EOPS-SW-10-0002, issue 1.0, date of issue 05 November 2010, available at <a href="http://cci.esa.int/filedepot_download/40/4">http://cci.esa.int/filedepot_download/40/4</a>  |
| [AD-2] | ESA Climate Change Initiative (CCI) Phase 1, Scientific User Consultation and Detailed Specification, Statement of Work, EOP-SEP/SOW/0031-09/SP, v1.4, 2009, available at <a href="http://www.esa-fire-cci.org/webfm_send/110">http://www.esa-fire-cci.org/webfm_send/110</a>               |
| [AD-3] | ESA Climate Change Initiative (CCI) Phase 2 Statement of Work, prepared by ESA Climate Office, Reference CCI-PRGM-EOPS-SW-12-0012, Issue 1.3, date of issue 24 March 2015, available at <a href="http://www.esa-fire-cci.org/webfm_send/828">http://www.esa-fire-cci.org/webfm_send/828</a> |
| [AD-4] | Phase 2 of the Climate Change Initiative (GMECV) Request for Quotation RFQ/3-14286/15/I-NB ECV Fire Disturbance, Proposal prepared by University of Alcalá (UAH, Spain) on July 24, 2015, in association with UAH's project partners.   |

### 1.4. Document Structure


Section 1 is the Executive Summary.

Section 2 is an introductory section.

Section 3 gives an overview of the pre-processing chain

Section 4 describes the MERIS BA algorithm.

Section 5 contains the references.

|   |  |  |       |                                     |      |
|---|--|--|-------|-------------------------------------|------|
|  | <b>Fire_cci</b><br><b>Algorithm Theoretical Basis</b><br><b>Document – MERIS</b> |  | Ref.: | Fire_cci_D2.1.1_YR1_ATBD-MERIS_v1.1 |      |
|   |  |  | Issue | 1.1                                 | Date |
|   |  |  |       | Page                                | 8    |

## 2. Introduction

### 2.1. Background

The ESA CCI initiative stresses the importance of providing a higher scientific visibility to data acquired by ESA sensors, especially in the context of the IPCC reports. This implies to produce consistent time series of accurate Essential Climate Variables (ECV) products, which can be used by the climate, atmospheric and ecosystem scientists for their modelling efforts. The importance of keeping long-term observations and the international links with other agencies currently generating ECV data is also stressed.

The Fire disturbance ECV identifies BA (BA) as the primary fire variable. Accordingly, the Fire\_cci project shall focus on developing and validating algorithms to meet GCOS ECV requirements for (consistent, stable, error-characterised) global satellite data products from multi-sensor data archives.

### 2.2. Purpose of the document

This document presents the theoretical basis of the algorithm developed to obtain burned area (BA) estimations from MERIS, including the pre-processing chain performed on the MERIS images. The current algorithm (version 4.1) builds on the experience acquired during the first phase of the Fire\_cci project, context in which the previous versions of the algorithm were developed. Further details on version 3.1, which was used to generate the 2006-2008 time series released in Phase 1 of the programme can be found on Alonso-Canas and Chuvieco (2015). These results were validated following a validation strategy described in Padilla et al (2015), and the final product was used by the climate research group to obtain relevant parameters for fire emission estimations and fire behaviour modelling (Chuvieco et al., 2016a).

Analysis of validation results for Fire\_cci v3.1 showed a tendency towards omission in the BA estimates. Therefore, the purpose of the current version was to diminish this tendency while keeping a similar commission error rate. Version 4.1 has been used to obtain the current product from years 2005 to 2011. The BA product is available at the CCI Data portal (details on [https://geogra.uah.es/fire\\_cci](https://geogra.uah.es/fire_cci), last access 29th July 2016).



### 3. Pre-processing Chain

#### 3.1. General overview

The completed automated Fire\_cci pre-processing chain of MERIS FRS performs the following operations (Figure 1): radiometric, geometric correction, pixel identification, atmospheric correction with aerosol retrieval as well as compositing and mosaicking. Improved algorithms were developed and validated for each of these pre-processing steps, which are detailed in Section 3.3.

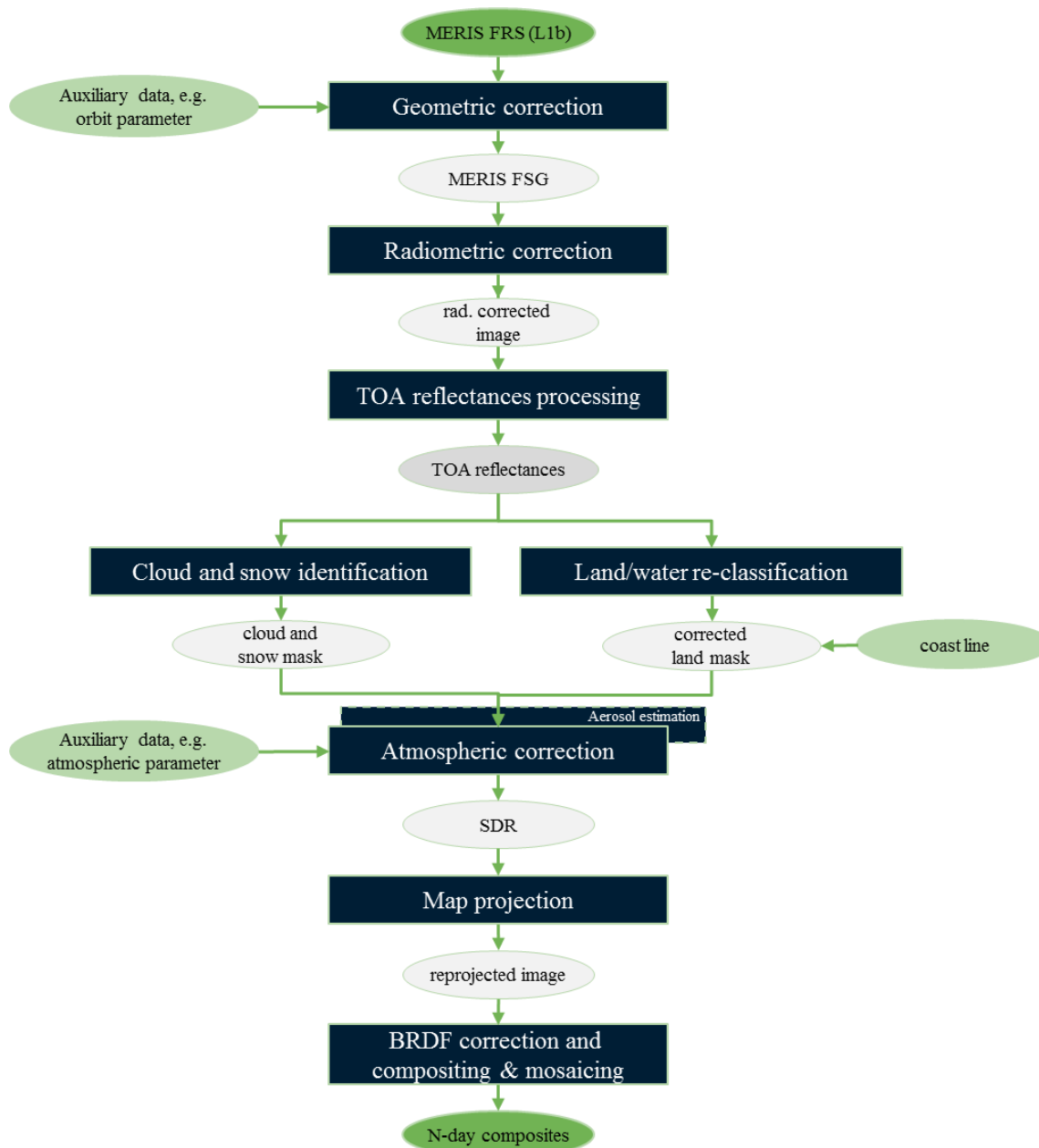


Figure 1: Schematic representation of the Fire\_cci pre-processing chain including input (pre-processing chain based on the GlobAlbedo and Land Cover CCI chain)

## 3.2. Quality Control of the input products

### 3.2.1. Methods

The quality control process of the input products in the Fire and Land Cover CCI projects comprises:

- automatic quality control;
- visual inspection of the input products which have been identified by the automatic quality control as erroneous products.

Furthermore, the quality control of the output products includes the visual inspection of the one-day surface reflectance (SR) composites and the inspection of time series.

For the internal quality assessment of MERIS FRS (L1b) products the following quality criteria have been defined:

- Format error – errors regarding the metadata, file format etc.
- Blank product - no lines with data
- Short product - products less than 7 seconds
- Duplicate product - products which have the same starting time (exact duplicate) and duration or which are temporarily and spatially included
- Missing data - few blank lines within the product
- Shifted geolocation - wrong geolocation, mainly caused by missing lines
- Horizontal and vertical stripes and wrong colours - one camera clearly different than the others, these errors often occur in combination with missing data and geolocation errors.
- Repetitive lines - repetition of lines in several locations of the product


All products which have not passed the internal Fire\_cci/LC\_cci quality control have been removed and cannot be used for the calculation of the one-day surface reflectance products. Additionally, the MERIS FRS products acquired during a special event (calibration, campaign or orbit manoeuvre) have also been removed from the data set by the internal Fire\_cci/LC\_cci quality control. The final data set is referred to as v2013.

### 3.2.2. Results

The following table summarizes the results of the internal Fire\_cci/LC\_cci QA for MERIS FRS from 2003-2013.

**Table 1 Results of the QA of MERIS FRS (L1b) from 2003-2012**

| Main Category    | Subcategory | Products | Relative |
|------------------|-------------|----------|----------|
| Potentially good |             | 135010   | 97.84%   |
| Corrupt          |             | 1456     | 1.06%    |
|                  | Short       |          | 719      |
|                  | Duplicate   |          | 462      |
|                  | Blank       |          | 275      |

|   |  |  |   |                 |
|---|--|--|---|-----------------|
|  | <b>Fire_cci</b><br><b>Algorithm Theoretical Basis</b><br><b>Document – MERIS</b> |  | Ref.: Fire_cci_D2.1.1_YR1_ATBD-MERIS_v1.1 |                 |
|   |  |  | Issue 1.1                                 | Date 11/11/2016 |
|   |  |  | Page 11                                   |                 |

| Main Category           | Subcategory | Products | Relative |
|-------------------------|-------------|----------|----------|
| Segregated <sup>1</sup> |             | 1522     | 1.10%    |
| Sum:                    |             | 137988   | 100%     |

### 3.3. Fire\_cci pre-processing chain

The complete automated pre-processing chain generates composites of surface reflectances of MERIS, by a series of pre-processing steps (Figure 1). Improved and new algorithms developed for each of these steps are presented in the sections below.

#### 3.3.1. Geometric correction

With AMORGOS (Accurate MERIS Ortho Rectified Geo-location Operational Software), ESA has made available a tool which improves MERIS FR geolocation better than 70m RMS. AMORGOS has been developed by ACRI-ST (Bourg and Etanchaud, 2007, Bourg et al., 2011a and 2011b). The updated AMORGOS 4.0 version was integrated in the pre-processing chain. AMORGOS 4.0 is not applicable to any other sensors by definition.

The investigation of the geolocation accuracy of the MERIS FSG and RRG revealed that the geometric accuracy of all products fulfils the Fire\_cci requirements.

#### 3.3.2. Radiometric Calibration

##### 3.3.2.1. MERIS calibration

Spectral and radiometric calibrations are key processes for all quantitative algorithms which exploit the spectral shape and magnitude. The spectral calibration of MERIS is performed by using measurements of a coloured diffuser and by a spectral matching technique using the measurements of the O2-A absorption band. The spectral calibration has been proved to be within 0.1nm accuracy. The radiometric accuracy is more critical. MERIS has two diffusers on-board, the first one being used regularly to monitor the radiometric response and the second one being exposed to sun light only 3 to 4 times per year in order to monitor the ageing of the first diffuser. With this technique, it was possible to derive a new degradation model of the instrument, which is applied for the 3<sup>rd</sup> reprocessing of Full Resolution products by ESA. This 3<sup>rd</sup> reprocessing quality is required for the Fire\_cci project.

##### 3.3.2.2. Coherent noise equalisation

The MERIS equalization module performs a radiometric equalisation of the MERIS L1b products. It reduces detector-to-detector and camera-to-camera systematic radiometric differences and results into a diminution of the vertical stripping observed on MERIS L1b products. The radiance at each pixel of a MERIS L1b products results from the measurements of 5 cameras spread across the swath, each one imaging a part of the swath with 740 so-called detectors in FR (corresponding to 185 mean detectors in RR). This results into 3700 detectors imaging the swath of MERIS FRS product (925 in

<sup>1</sup> Segregated products contain errors which probably will be recovered on a later stage with suitable tools or they are only partially affected by errors. These products have been removed from the MERIS FRS Fire\_cci/LC\_cci data set.

|   |  |  |       |                                     |      |            |
|---|--|--|-------|-------------------------------------|------|------------|
|  | <b>Fire_cci</b><br><b>Algorithm Theoretical Basis</b><br><b>Document – MERIS</b> |  | Ref.: | Fire_cci_D2.1.1_YR1_ATBD-MERIS_v1.1 |      |            |
|   |  |  | Issue | 1.1                                 | Date | 11/11/2016 |
|   |  |  |       |                                     | Page | 12         |

RR). The response of each one of these detectors is calibrated during the routine operation of the instrument. Residual uncertainties in the calibration process result into detector-to-detector and camera-to-camera systematic radiometric differences. The equalisation corrects for these radiometric differences via a set of detector dependant coefficients correcting for the residual uncertainties in the calibration process. These coefficients are retrieved via a methodology described by Bouvet and Ramoino (2010), based on observations of the Antarctica plateau spread out throughout the MERIS mission lifetime.

### 3.3.2.3. Smile correction

MERIS measures reflected sun light using a CCD detector. The CCD measures in one of its dimensions one image line, and in the other dimension the spectrally dispersed radiance for each pixel along the image line. I.e., the spectral measurements of each pixel along an image line are made by its own set of sensors of the CCD. This causes small variations of the spectral wavelength of each pixel along the image. This is called the "smile effect".

The MERIS instrument is composed of 5 cameras, each equipped with its own CCD sensor. The variation of the wavelength per pixel is in order of 1nm from one camera to another, while they are in the order of 0.1nm within one camera.

Even though this variation is small compared to the spectral bandwidth of a band, which is typical 10nm, and can hardly be seen in an image, it can cause disturbances in processing algorithms which require very precise measurements, for example the retrieval of chlorophyll in the ocean. These disturbances can result in visual artefact ("camera borders") or reduced accuracy of retrieved Level 2 products, e.g. surface reflectance products. The MERIS FRS (L1b) product is not smile corrected, because this product shall provide the user exactly what the instrument is measuring, and that is in fact the radiance at the given wavelength of each pixel. Therefore, the Fire\_cci/LC\_cci pre-processing chain includes the correction of the smile effect as part of the radiometric calibration.

### 3.3.3. Land water delineation and cloud screening - pixel identification

The Multi Sensor Pixel Identification approach (which is also applied in the Land Cover CCI project) classifies each pixel to be processed according to a series of pixel categories, which include cloud and cloud shadow, clear-land, clear-water and clear-snow/ice. Cloudy pixels are not processed in Fire\_cci project, while land, water and snow pixels must be distinguished because of the particular processing steps associated to each surface type. In particular, water pixels must be separated from land surfaces even in the case of continental water bodies, as these are flagged in the final pre-processed product. Snow and snow-free surfaces will also be considered separately in the final pre-processed product.<sup>2</sup>

<sup>2</sup> The Fire\_cci BA processing requires only the discrimination in burnable and non-burnable, but as mentioned before, the following pre-processing steps require the discrimination in the categories - cloud and cloud shadow, clear-land, clear-water and clear-snow. For example, the used aerosol retrieval method is only applicable over clear land pixel without snow/ice coverage.

### 3.3.3.1. Pixel identification

While the information if a pixel is over water or land can be taken from a static map as a good first guess, provided the geo-location of the pixel is better than the size of the pixel, the cloud coverage is spatially and temporally highly variable and needs to be derived from the measurement itself. Also, the snow coverage can be spatially and temporally variable and is therefore also derived from the measurements itself. After knowing whether a pixel is cloudy or clear, in the clear sky case the land-water information can be refined using the measurement. This is particularly necessary in the coastal zone where the actual land-water boundary changes due to tides, when the pixel size is small enough to resolve this difference. Also maps are not always correct so that a radiometric refinement is advisable.

A big problem is the distinction between clouds and snow/ice, in particular for instruments which do not have spectral bands in the NIR and SWIR. An extensive study including the cloud screening over snow and ice has been undertaken (Aoki et al., 2007; Hori et al., 2007; Stamnes et al., 2007). Snow and ice are less reflective in the NIR spectral region, and the so called normalized differentiation ice index (NDII) and the corresponding snow index (NDSI) are good tools to differentiate clouds from snow and ice. These indices are defined as follows<sup>3</sup>:

$$NDII = \frac{R(0.545\mu m) - R(1.050\mu m)}{R(0.545\mu m) + R(1.050\mu m)}; NDSI = \frac{R(0.545\mu m) - R(1.640\mu m)}{R(0.545\mu m) + R(1.640\mu m)}$$

eq. 3.1

The reflectance for ice decreases with the wavelength must faster as compared to snow. Therefore, large values of NDII signify the bare ice case.

### 3.3.3.2. Practical consideration

The Fire\_cci pixel identification is a classification for the MERIS FRS data considered. The uniqueness consists of a certain set of features, which are calculated for each instrument and decision tree as well as probabilistic combination of these features in order to calculate a set of pixel classification attributes. The implementation of how the features are calculated is instrument specific. This approach has the advantage to be easily extendable to other instruments, and it is also applied in the Land Cover CCI project as well as in the GlobAlbedo project, where additionally AATSR is used.

The following features (Table 2) are used in the probabilistic combination, including how they are calculated for the MERIS instrument.

**Table 2: Feature - Pixel identification<sup>4</sup>**

| Feature  | Explanation   |
|----------|---|
| Pressure | Indicating a high altitude from where the photons are scattered. Can be derived from measurements in gaseous absorption bands, e.g. O2A or water vapour |

<sup>3</sup> The NDSI definition has been updated for the MERIS sensor (MDSI) - see the Table 3.

<sup>4</sup> Some features like temperature information are not available from MERIS, but they are included as a key feature in the overall approach; temperature is generally a very powerful criterion for cloud detection.

| Feature                 | Explanation  |
|-------------------------|--|
| NDVI                    | A high vegetation index is an indication of a (semi-) transparent atmosphere   |
| NDSI                    | The NDSI is a meaningful quantity only above bright surfaces. Then it can be used to separate snow/ice from clouds (see footnote number 3).  |
| White                   | A bright and spectrally flat signal; can be a cloud or snow/ice  |
| Spectral Flatness       | A spectrally flat signal; the colour can be anything from black over grey to white.  |
| Temperature             | Temperature of the emitting surface; clouds can be very cold.  |
| Bright                  | Brightness of the scattering surface   |
| Glint Risk              | The glint risk can be calculated from the observation geometry and wind speed, assuming a certain wave distribution (e.g. Cox and Munk, 1954). Glint and clouds are hardly separable and hence it is useful to identify glint risk in addition with the cloud/water classification. <sup>5</sup> |
| Radiometric Land Value  | A classification of the surface type as land, provided that the pixel is clear and the measurement can be used to assess the surface type.   |
| Radiometric Water Value | A classification of the surface type as water, provided that the pixel is clear and the measurement can be used to assess the surface type.  |
| A priori Land Value     | Classification of the pixel using a static background map and the geolocation of the pixel.  |
| A priori Water Value    | Classification of the pixel using a static background map and the geolocation of the pixel.  |

The feature definition for MERIS is shown in Table 3. The index used in array notation below is starting with 0.

**Table 3: Feature Definition for MERIS<sup>6</sup>**

| Feature  | MERIS  | Comment   |
|----------|--|---|
| Pressure | <pre> if (isLand())   press_value = (p<sub>baro</sub> - p1)/1000.0; else if (isWater())   press_value =(p<sub>baro</sub> - p<sub>scatt</sub>)/1000.0; </pre> | p1 and pscatt are apparent pressure products,. p <sub>baro</sub> is the barometric pressure. (Santer and Aznay, 2008) |
| NDVI     | <pre> value = brr[b753]-brr[b620]/ (brr[b753]+brr[b620]) </pre>  | brr is the reflectance corrected for gaseous absorption and Rayleigh scattering                                       |

<sup>5</sup> Fire\_cci does not require atmospheric correction over water bodies; this implies no cloud detection over water, which is problematic under sun glint conditions.

<sup>6</sup> Not every key feature can be calculated for every instrument. In such cases the key feature value is constant equal to 0.5. This convention allows formulating the logical combination of key features even if a feature is not available for the instrument, and hence the logical combination for other instruments can be easily adapted to the selected instrument.



| Feature                 | MERIS  | Comment  |
|-------------------------|--|--|
| NDSI                    | $\text{value} = \frac{\text{brr}[b865] - \text{brr}[b885]}{(\text{brr}[b865] + \text{brr}[b885])}$   | Adaption of the NDSI to MERIS NDSI (MDSI) as proposed by the MERIS Global Land Surface Albedo MAPS project (Preusker et al., 2008)   |
| White                   | <pre>if (brightValue() &gt; BRIGHT_FOR_WHITE_THRESH)   white_value = spectralFlatnessValue(); else   white_value = 0;</pre>  |  |
| Spectral Flatness       | <pre>slope0 = spectralSlope(brr[b412], brr[b490]) slope1 = spectralSlope(brr[b560], brr[b620]) slope2 = spectralSlope(brr[b665], brr[b753]) spectralFlatness = 1.0f - Math.abs(1000.0 * (slope0 + slope1 + slope2) / 3.0);</pre> |  |
| Temperature             | 0.5  |  |
| Bright                  | $\text{bright\_value} = \frac{\text{brr}[b442]}{(6.0 * \text{brr}442\text{Thresh})}$   | brr442Thresh is a value read from a LUT; the LUT is a theoretical maximal reflectance for a given geometry and a bright land surface. It has been calculated by R. Santer and is available from the auxiliary data of the MERIS operational processor (Zagolski and Goryl, 2011) |
| Glint Risk              | Shall be calculated from geometry and wind speed from tie points. Not available in used IDEPIX version   | currently set to FALSE   |
| Radiometric Land Value  | <pre>if   refl[b753] &gt;= refl[620] &amp;&amp; refl[620] &gt; refl620_Land_Thresh     radiom_land_value = 1.0 else   radiom_land_value = 0.5</pre>  | in case of cloudy pixel: radiom_land_value = 0.5   |
| Radiometric Water Value | <pre>if   refl[b753] &lt; refl[620] &amp;&amp; refl[620] &lt; refl620_Water_Thresh     radiom_water_value = 1.0 else   value = 0.5</pre>   | in case of cloudy pixel: radiom_water_value = 0.5  |

| Feature              | MERIS  | Comment |
|----------------------|--|---------|
| A priori Land Value  | <pre>if (l1FlagLand)   return 1.0f; else   return 0.0f;</pre>  |         |
| A priori Water Value | <pre>if (!l1FlagLand)   return 1.0f; else   return 0.0f;</pre> |         |

The classification attributes shown in Table 4 (binary values, also named flags) are derived from the features with given logic. This logic is no longer instrument dependent.

**Table 4: Processing logic**

| Classification attribute | Definition  | Comment   |
|--------------------------|---|---|
| isCloud                  | <pre>return (whiteValue() + brightValue() + pressureValue() + temperatureValue() &gt; CLOUD_THRESH &amp;&amp; !isClearSnow())</pre>   | The final binary cloud flag. A pixel is either Cloud, ClearLand or ClearWater or ClearSnow  |
| isClearSnow              | <pre>return (isBrightWhite() &amp;&amp; ndsiValue() &gt; NDSI_THRESH)</pre>   | isBrightWhite is defined below  |
| isClearLand              | <pre>if (radiometricLandValue() != 0.5)   landValue = radiometricLandValue(); else if (aPrioriLandValue() &gt; 0.5)   landValue = aPrioriLandValue(); else   return false; // this means: if we have no information about land, we return isClearLand = false return (!isCloud() &amp;&amp; landValue &gt; LAND_THRESH)</pre>           | If a radiometric land value is available, i.e. it is not the uncertainty value of 0.5, than this is used in the subsequent test. Otherwise the a priori land value is used in the test. The test simply compares the value with a threshold. The choice of the threshold depends on the user. If he wants to be really sure he should use a value close to 1. |
| isClearWater             | <pre>if (radiometricWaterValue() !=0.5)   waterValue = radiometricWaterValue(); else if (aPrioriWaterValue() &gt; 0.5)   waterValue = aPrioriWaterValue(); else   return false; // this means: if we have no information about water, we return isClearWater = false return (!isCloud() &amp;&amp; waterValue &gt; WATER_THRESH);</pre> | same logic as for the ClearLand test  |



| Classification attribute | Definition   | Comment  |
|--------------------------|--|--|
| isBrightWhite            | return (whiteValue() + brightValue() > BRIGHTWHITE_THRESH) | A pixel that has one of the two characteristics, bright or white, has a potential to be cloudy. The stronger both features are the higher the probability. |
| isLand                   | return (aPriorilandValue() > LAND_THRESH)                  | This is the surface type of the pixel, regardless if it is snow covered or if a cloud is above during measurement.   |
| isWater                  | return (aPrioriWaterValue() > WATER_THRESH)                |  |
| isBright                 | return (brightValue() > BRIGHT_THRESH)                     | These tests map the real values of the features to binary flags  |
| isWhite                  | return (whiteValue() > WHITE_THRESH)                       |  |
| isCold                   | return (temperatureValue > TEMPERATURE_THRESH)             |  |
| isVegRisk                | return (ndviValue() > NDVI_THRESH)                         |  |
| isGlintRisk              | return (glintRiskValue > GLINT_RISK_THRESH)                |  |
| isHigh                   | return (pressureValue() > PRESSURE_THRESH)                 |  |

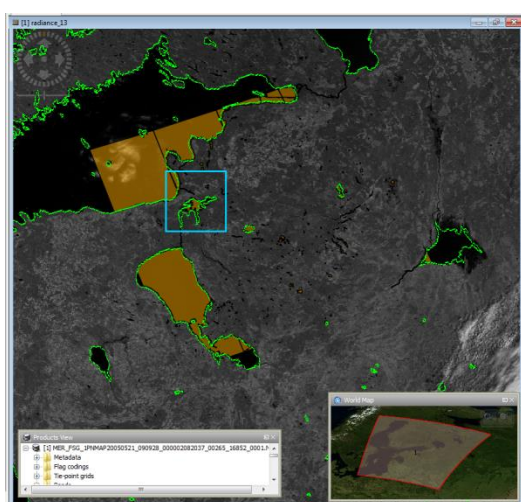
Table 5 lists the nominal values for the scalar thresholds.

**Table 5: Thresholds**

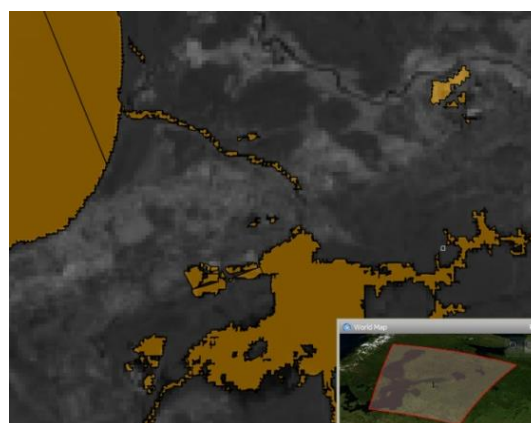
| Threshold               | MERIS Value |
|-------------------------|-------------|
| BRIGHTWHITE_THRESH      | 1.5         |
| NDSI_THRESH             | 0.68        |
| PRESSURE_THRESH         | 0.9         |
| CLOUD_THRESH            | 1.65        |
| UNCERTAINTY_VALUE       | 0.5         |
| LAND_THRESH             | 0.9         |
| WATER_THRESH            | 0.9         |
| BRIGHT_THRESH           | 0.25        |
| WHITE_THRESH            | 0.9         |
| BRIGHT_FOR_WHITE_THRESH | 0.8         |
| NDVI_THRESH             | 0.7         |
| TEMPERATURE_THRESH      | 0.9         |

The a priori Land Value and the a priori Water Value are determined by a static background map as well as the geo-location of the corresponding pixel. The SRTM SWBD map is used in the project from [http://dds.cr.usgs.gov/srtm/version2\\_1/SWBD/](http://dds.cr.usgs.gov/srtm/version2_1/SWBD/). Figure 2 shows the MERIS FRS (L1b) coastline (green) as indicator of the MERIS FRS (L1b) and the application of the new SRTM SWBD map (brown). The improvement is clearly visible.

For a further refinement of the static land/water classification, the Land Cover CCI SAR water body product (Ph2\_ATBDv1.1, 2016) has been developed and the assessment of the suitability is currently ongoing. Therefore, this product is not applied in the pixel identification as static background map at the moment, and will be evaluated for Year 2 of the project.



MERIS image and subset region (blue), and L1b coastline (green)



MERIS subset image and SRTM SWBD map (brown)

Product:  
 MER\_FSG\_1PNMAP20050521\_090928\_00000208  
 2037\_00265\_16852\_0001.N1

**Figure 2: Original MERIS FRS L1b coastline - green, SRTM SWBD Land/water map - brown**


### 3.3.3.3. Adaptation of IdePix

The assessment of MERIS FR products using the former IdePix shows that the data quality has not yet reached the expected level, mainly due to clouds. A better pixel classification with respect to the class “clear land” is required. Therefore new pixel identification features for the Land Cover CCI and Fire\_cci processing have been developed and applied.

Temporal Features: an improvement of pixel identification is accessible by analysing their temporal characteristics. Based on this approach a temporal filter has also been applied and is described in detail in the Section 3.3.5.2.

Spectral Features: the following new spectral features have been considered, investigated und applied:

- *blue band feature:* the blue band feature based on the Blue Band Cloud Screening of the GlobCover Project and the entire description may be found in the GlobCover Design Justification File (GlobCover\_DJFv3.8, 2008). A simple blue band test has been adopted for MERIS by using the 412 nm channel. The developed cloud

|   |  |  |       |                                     |      |            |
|---|--|--|-------|-------------------------------------|------|------------|
|  | <b>Fire_cci</b><br><b>Algorithm Theoretical Basis</b><br><b>Document – MERIS</b> |  | Ref.: | Fire_cci_D2.1.1_YR1_ATBD-MERIS_v1.1 |      |            |
|   |  |  | Issue | 1.1                                 | Date | 11/11/2016 |
|   |  |  |       |                                     | Page | 19         |

screening method is applied to reflectances. A first threshold for band 1 reflectances is used to detect the most brilliant dense clouds. The clear pixels are tested by a filter which performs the reflectance ratio of band11 and band10 related to the altitude of the scattering surface. An optimised threshold permits identifying thin clouds which are not detected by the first blue band test. Three states are supposed: 0=Out of Orbit, 1=Clear and 2=Cloud. The optimised cloud mask is globally coherent with the bright flag of standard MERIS products. However, a higher performance of the cloud screening over semi-transparent clouds can be observed. Large areas are not detected by the bright flag or probability algorithms. The analysis shows that the blue band algorithm is more able to detect semi-transparent clouds.


- *cloud value feature*: the cloud value feature is predicted by two neuronal network models or to put it more succinctly, they are back-propagation neuronal networks with one input and one output layer. The neuron nets (NNs) have been trained with a back-propagation learning algorithm by using the PixBox data whereas the training dataset was split with respect to the surface properties land and water and these two datasets have been used separately for the training. Therefore we get a so-called LandNN and a WaterNN for the prediction of the cloud value. The PixBox data are described in the PVASR (Ph1\_PVASRv2.0, 2012). The decision of which NN will be used only depends on the classified surface type through IdePix. Afterwards the cloud value is calculated through the NN by using the MERIS FSG TOA reflectance spectrum as input. The cloud value has a range from 0 through 2. The user defined thresholds 1.25 for the LandNN and 1.35 for the WaterNN are used for the verification of the current pixel status as clear land or clear water. If the cloud value is greater than the particular threshold then the pixel status is set to cloud.
- *clear land feature*: the clear land feature of pixel identification is based on the analysis of the spectral characteristics in the HSV (Hue Saturation Value) - colour space. The clear land feature is described in detail in the Section 3.3.5.1. So far, this feature is only applicable to MERIS data. The adaptation to other sensors would require a determination of the prior probability and the definition of thresholds regarding the considered sensors.

#### 3.3.3.4. Error budget estimates

The adaption of IdePix by including the new features has influenced the error estimation. Now the error cannot simply be calculated automatically by probabilistic arithmetic. Therefore, as a first guess we will introduce a measure of certainty that the inspected pixel is covered by a cloud. This measure of certainty for each pixel is calculated by counting the number of the true cloud features, and a pixel is considered cloudy if the measure of certainty is very high.

#### 3.3.3.5. Cloud shadow and cloud edge detection

A more comprehensive representation of clouds is provided by two additional pixel properties, ‘cloud edge’ and ‘cloud shadow’. These two properties are also kept in the pixel identification flag and can be considered as a kind of “post-processing” in the cloud detection.

|   |  |       |                                     |      |            |    |
|---|--|-------|-------------------------------------|------|------------|----|
|  | <b>Fire_cci</b><br><b>Algorithm Theoretical Basis</b><br><b>Document – MERIS</b> | Ref.: | Fire_cci_D2.1.1_YR1_ATBD-MERIS_v1.1 |      |            |    |
|   |  | Issue | 1.1                                 | Date | 11/11/2016 |    |
|   |  |       |                                     |      | Page       | 20 |

To detect dark cloud shadow pixels -whose spectra are polluted by the shadow- the position of the shadow is determined by projecting the ‘cloud pixels’ onto the ground using the sun position, the pixel’s altitude on Earth, and the cloud height estimated from cloud top pressure (Figure 3).



**Figure 3: Cloud, cloud edges and cloud shadow**

Cloud edge pixels are in principle regarded as neighbour pixels of a ‘cloud’ as identified before in the pixel classification. The width of this edge (in number of pixels) can be set by the user. Briefly, the algorithm to identify cloud edge pixels works as follows:

- use a 2x2 square with reference pixel in upper left
- move this square row-by-row over the given tile
- if reference pixel was not cloud, don't do anything
- if reference pixel is cloudy:
  - if 2x2 square only has cloud pixels, then set cloud buffer of two pixels in both x and y direction of reference pixel;
  - if 2x2 square also has non-cloudy pixels, do the same but with cloud buffer of only 1.

The improvement of Phase 2 algorithms of the Fire\_cci project includes also the improvement of the cloud shadow detection. The algorithm contains three main parts which are explained in the following paragraphs. The results of the individual steps are presented visually for a better comprehension (see Figure 4).

- Step 1: Cloud top height (CTH) and cloud base height (CBH) estimation
  - CTH: Use temperature (MODIS, Landsat, AVHRR) or O<sub>2</sub> absorption (MERIS) to estimate CTH, Otherwise set CTH=12km (SENTINEL 2)
  - CBH: Use constant CBH=0 or  $CBH = \min_{\text{window}}(CTH)$  window = n x n pixel array
- Step 2: potential cloud shadow area identification
  - Intersection of line-of-sight with cloud
  - Identify connected potential cloud shadow areas (seed-growing algorithm)
- Step 3: cloud shadow identification
  - for each connected cloud shadow area perform k-means cluster analysis with k = 4 clusters

- Add local variance as additional feature into clustering for high spatial resolution sensors (shadow areas are less contrasted)
- Sort clusters into either clear and cloud shadow

In case of the shadow detection for MERIS only step 1 and step 2 have been applied.

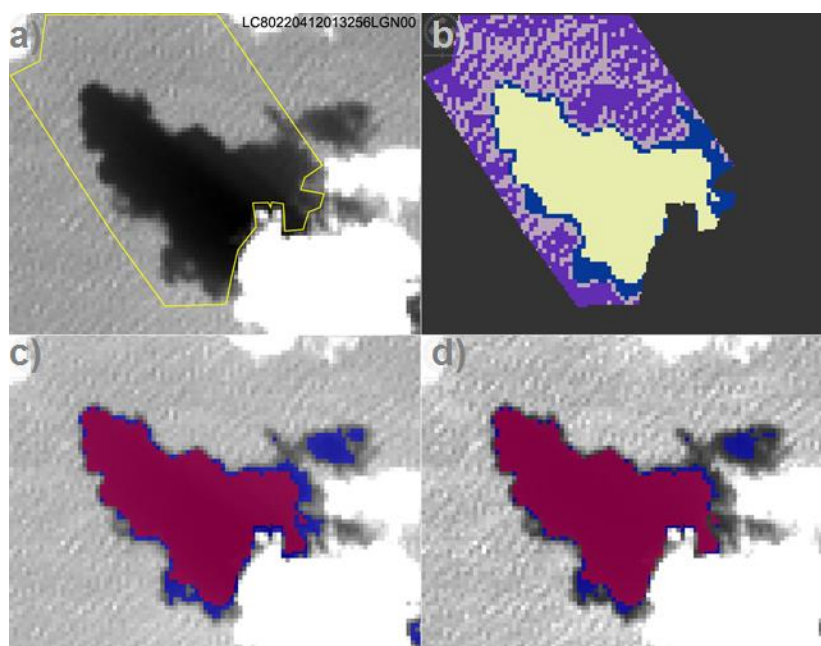



**Figure 4: Breadboard cloud shadow algorithm - here shown on a Landsat image a) blue channel with cloud shadow potential area border for the biggest cloud yellow) b) k-means cluster analysis result for this cloud c) blue channel with cloud shadow for this cloud d) SWIR channel with cloud shadow for both clouds**

### 3.3.4. Atmospheric correction - aerosol and spectral directional reflectance retrieval

The atmospheric correction includes the correction for the absorbing and scattering effects of atmospheric gases, in particular ozone, oxygen and water vapour, of the scattering due to air molecules (Rayleigh scattering) and aerosol particles. All components except aerosols can be rather easily corrected. Ozone can be taken from other satellites, available from meteorological services, and oxygen and water vapour can be taken from sensor measurements thanks to dedicated spectral bands or can be taken also from meteorological data sets, e.g. ERA Interim data set. However, aerosols are spatially and temporally highly variable and do not have distinct spectral absorption features, so they cannot be measured easily from MERIS measurements. Techniques exist to derive aerosol information from measurements where the surface signal is low, but the areas where the surface is dark enough are sparse and spatial-temporal interpolation is necessary. Also, these derived aerosols optical properties are connected with a substantial error. The aerosol correction is the largest contributor to the error of the atmospheric correction. The challenge in Fire\_cci is to minimize this error and to quantify it reliably. The method should ideally work across different instruments.

The aerosol correction typically consists of two parts: the calculation of these aerosol properties and secondly the actual correction of the reflectance (after Rayleigh and gas absorption correction). This can be a sequential process where the reflectance correction

|   |  |  |       |                                     |      |            |
|---|--|--|-------|-------------------------------------|------|------------|
|  | <b>Fire_cci</b><br><b>Algorithm Theoretical Basis</b><br><b>Document – MERIS</b> |  | Ref.: | Fire_cci_D2.1.1_YR1_ATBD-MERIS_v1.1 |      |            |
|   |  |  | Issue | 1.1                                 | Date | 11/11/2016 |
|   |  |  |       |                                     | Page | 22         |

takes an aerosol optical depth and its spectral dependency as input, or a one-step approach where aerosol properties and reflectance corrections are one implicit step. An approach for retrieval of aerosol properties for MERIS has been developed by the University Swansea for the GlobAlbedo project. It is based on an inverse modelling approach, working on a larger area of 8 x 8 km to estimate the aerosol properties, which is then used to correct each single pixel. This method provides significantly more aerosol retrievals than the LARS method (Santer and Ramon, 2011), which is the baseline for the GlobCover aerosols.

The aerosol retrieval was developed under the GlobAlbedo project for Surface Directional Reflectance (SDR) estimation by the Institute for Space Sciences, Free University of Berlin; fully documented in GlobCover\_DJFv3.8 (2008) and an improved version documented in GlobAlbedo\_ATBDv4.12 (2013). Here we give a brief summary of points relevant to aerosol estimation. The algorithm was designed to produce SDR (including uncertainties) from top of atmosphere (TOA) radiance data. The algorithm requires the inputs from the pixel classification and atmospheric condition parameters, e.g. aerosol properties. The iterative retrieval of atmospheric aerosol requires a fast approximation of atmospheric radiative transfer, to relate TOA to surface reflectance for varying aerosol loading.

To retrieve estimates of aerosol properties from measured satellite radiances, we need to solve the inverse problem to separate the atmospheric and surface scattering contributions to the observed signal. This normally requires some assumptions to be made on the land surface brightness. The aerosol properties for MERIS have been retrieved by the aerosol retrieval method developed by the University Swansea for the GlobAlbedo project. Within the proposed framework, these assumptions are expressed as constraints defined by error of fit to a parameterized model describing the surface angular or spectral reflectance. For the single view instruments we apply constraints based on the dark object method (DOM).

The aerosol retrieval includes the calculation of the aerosol optical depth (AOD). Estimates of aerosol extinction are needed for the conversion from top-of-atmosphere measurements to surface reflectance. Aerosol optical depth and aerosol model plus an estimate of the uncertainty in AOD are derived by the Aerosol Retrieval processor from every data set to be processed. It must be noted that AOD and aerosol model are assumed to sufficiently account for the variability in the atmospheric conditions to calculate these terms, while water vapour and ozone column contents are needed in addition to aerosol parameters in order to retrieve the most accurate Lambertian equivalent reflectance. All other atmospheric constituents are just set to climatology values in the algorithm. This selection is justified by the relatively higher impact of aerosol extinction in the spectral channels of MERIS and SPOT-VGT instruments, particularly in the visible spectrum.

The problem of surface reflectance and aerosol retrieval can essentially be formulated as one of multivariate optimisation subject to multiple constraints:

- Given a set of satellite TOA reflectance and an initial guess of atmospheric profile, the corresponding set of surface reflectance is estimated
- Application of the observed set to the estimated set of reflectance results in an error metric, where a lower value of the metric corresponds to a set of surface reflectance (and hence atmospheric profile) that is more realistic

|   |                                    |  |   |            |
|---|------------------------------------|--|---|------------|
|  | <b>Fire_cci</b>                    |  | Ref.: Fire_cci_D2.1.1_YR1_ATBD-MERIS_v1.1 |            |
|   | <b>Algorithm Theoretical Basis</b> |  | Issue                                     | 1.1        |
|   | <b>Document – MERIS</b>            |  | Date                                      | 11/11/2016 |
|   |                                    |  | Page                                      | 23         |

These two steps are repeated with refined atmospheric profiles until convergence at an optimal solution. It consists of the following steps:

- Atmospheric correction of averaged TOA radiance using an estimate of aerosol optical thickness. The resulting estimate of surface reflectance for each input channel is calculated by means of lookup tables. Besides the aerosol optical depth the atmospheric correction depends on the aerosol model, viewing and illumination geometry, surface pressure, and ozone content
- Error metric calculation
- Optimisation of the estimated aerosol optical thickness by means of minimisation of the error metric as implicit function of aerosol optical thickness.
- The implicit dependency of aerosol optical thickness is given by the surface reflectance estimated in Step 1

The algorithm components are therefore: (i) design of an efficient and accurate scheme for deriving surface reflectance for known atmospheric profile, and (ii) formulation of constraints on the land surface reflectance suitable spectral sampling of the instruments used. The method is applied to estimate aerosol at a more coarse spatial resolution (8x8 km) than the underlying surface reflectance, and a subsequent interpolation step is used to obtain per-pixel values.

The TOA reflectance or apparent spectral directional reflectance  $R_{\lambda}^*$  in the waveband  $\lambda$  of the coupled surface-atmosphere system is related to the radiance  $L_{\lambda}$  measured by a satellite at the TOA by:

$$R_{\lambda}^*(\Omega_s, \Omega_v) = \frac{\pi L_{\lambda}(\Omega_s, \Omega_v)}{\mu_s E_{s,\lambda}} \quad \text{eq. 3.2}$$

where  $E_{s,\lambda}$  is the extraterrestrial irradiance at the time of the measurement. The solar and view vectors are denoted by  $\Omega_s$  and  $\Omega_v$  respectively, while  $\mu_s$  and  $\mu_v$  denote cosines of solar and view zenith.

A uniform, Lambertian surface is normally assumed as a basis for the modelling of the atmosphere-surface radiative transfer for operational atmospheric correction algorithms of single-view instruments. Under that assumption, the relationship between top of atmosphere reflectance  $R_{\lambda}^*$  and the surface directional reflectance  $R_{\lambda}$  can be approximated by the equation:

$$R_{\lambda}^*(\Omega_s, \Omega_v) = R_{atm,\lambda}(\Omega_s, \Omega_v) + \gamma_{\lambda}(\mu_s)\gamma_{\lambda}(\mu_v) \frac{R_{\lambda}}{1 - \bar{\rho}_{\lambda} R_{\lambda}} \quad \text{eq. 3.3}$$

Where  $R_{atm,\lambda}$  means the atmospheric scattering term (TOA reflectance for zero surface reflectance),  $\gamma_{\lambda}$  denotes atmospheric transmission for either sensor to ground or ground to sensor for waveband  $\lambda$ , and  $\bar{\rho}_{\lambda}$  denotes atmospheric bi-hemispherical albedo with respect to the surface. The solar and view vectors are denoted by  $\Omega_s$  and  $\Omega_v$  respectively, while  $\mu_s$  and  $\mu_v$  denotes denote cosines of solar and view zenith. Spectral directional reflectance  $R_{\lambda}$  is derived from TOA reflectance by means of the analytical inversion of eq. 3.4, and the corresponding equation is:

$$R_{\lambda}(\Omega_s, \Omega_v) = \frac{R_{\lambda}^*(\Omega_s, \Omega_v) - R_{atm,\lambda}(\Omega_s, \Omega_v)}{\gamma_{\lambda}(\mu_s)\gamma_{\lambda}(\mu_v) + \bar{\rho}_{\lambda} [R_{\lambda}^*(\Omega_s, \Omega_v) - R_{atm,\lambda}(\Omega_s, \Omega_v)]} \quad \text{eq. 3.4}$$

|   |  |  |       |                                     |      |            |
|---|--|--|-------|-------------------------------------|------|------------|
|  | <b>Fire_cci</b><br><b>Algorithm Theoretical Basis</b><br><b>Document – MERIS</b> |  | Ref.: | Fire_cci_D2.1.1_YR1_ATBD-MERIS_v1.1 |      |            |
|   |  |  | Issue | 1.1                                 | Date | 11/11/2016 |
|   |  |  |       |                                     | Page | 24         |

As discussed in GlobAlbedo\_ATBD/BBDRv1.0 (2010) and in GlobAlbedo\_ATBDv4.12 (2013), the Lambertian equivalent reflectance  $R_\lambda$  derived from eq. 3.4, which is taken as SDR in the GlobAlbedo processing chain, represents a smoothed version of the surface BRDF, with errors up to 15% for turbid atmospheres (Hu et al., 1999).

$R_\lambda^*$  is calculated from TOA radiance with eq. 3.2 and first corrected from gaseous absorption with a look-up table for a set of input AMF, CWV and OZO. AMF and CWV are considered pixel-wise, while a mean value representative of the imaged area is used for OZO. The atmospheric parameters  $R_{atm,\lambda}$ ,  $\gamma_\lambda$  and  $\bar{\rho}_\lambda$  are provided by a look-up table per pixel, with the input VZA, SZA, RAA, ELEV and AOD550 also provided on a per-pixel basis. No correction of adjacency effects (Mekler and Kaufman, 1982; Kaufman, 1989) has been found to be necessary.

The look-up tables intended for aerosol and SDR retrieval and for error propagation have been compiled with the Matrix-Operator-Model (MOMO) radiative transfer code (Fischer and Grassl, 1984; Fell and Fischer, 2001). MOMO is a widely accepted radiative transfer code which provides all the features required for atmospheric radiative transfer simulations in the Fire\_cci project. The look-up tables intended for gas correction and also for error propagation for are calculated with the 6S (Second Simulation of the Satellite Signal in the Solar Spectrum) radiative transfer code (Vermote et al., 1997a and 1997b). This code is intended for fast radiative transfer calculations at a relatively coarse internal spectral sampling of 2.5 nm.

Tracking of uncertainties is one of the specific requirements for the Fire\_cci processing. The purpose in this part of the processing is to generate a reliable estimation of the errors in the SDR products including the error covariance between the different spectral ranges. Different error sources are considered: instrumental noise, atmosphere and directional reflectance effects. The uncertainty of the SDR values can be propagated as one of the source uncertainties in the BA processing. Alternatively, it can be used in a Monte-Carlo approach, including ensemble building, to determine the output parameter uncertainty in the BA processing.

$$\begin{aligned}
 & \text{for } j = 1 \dots N_\lambda \text{ and } N_{obs} := N_{obs,STATUS_X} \quad \Delta S_{agg} := \\
 & \Delta SDR_{MIN(SDR(MERIS\_BAND\_14(j;N_{obs}))}
 \end{aligned}
 \tag{eq. 3-5}$$


### 3.3.5. Clear land filtering

#### 3.3.5.1. Clear land feature of IdePix

An important step before or in the compositing algorithm is the application of the clear land feature, which was developed to deal with a significant amount of residual clouds and haze not detected by the other IdePix features and which are thus present in the L2 products. The clear land feature is applied to all pixels classified as “clear land” by IdePix. The steps of this clear land pixel filter applied to each pixel of the SDR image can be summarized as follows:

- Conversion from RGB to HSV



|   |  |  |       |                                       |      |            |
|---|--|--|-------|---------------------------------------|------|------------|
|  | <b>Fire_cci</b><br><b>Algorithm Theoretical Basis</b><br><b>Document – MERIS</b> |  | Ref.: | Fire_cci_D2.1.1.1_YR1_ATBD-MERIS_v1.1 |      |            |
|   |  |  | Issue | 1.1                                   | Date | 11/11/2016 |
|   |  |  |       |                                       | Page | 25         |

- Retrieval of probability of land and cloud based on prior probability densities of each class
- Application of thresholds to a combination of the retrieved probability of land and cloud<sup>7</sup>

This algorithm is based on surface reflectance values (i.e. on the final L2 products, just before the re-projection and compositing steps).

### 3.3.5.2. Temporal filtering

An important step in the compositing algorithm is the temporal pixel classification, which was developed to deal with a significant amount of residual clouds and haze not detected by IdePix and the clear land filter and which are thus present in the L2 products. The temporal pixel classification amounts to a temporal filtering. It is applied to all pixels classified as “clear land” by IdePix and consists in computing the mean  $\mu$  and standard deviation  $\sigma$  of the MERIS band 8  $\rho_8$  over a certain time interval. This time interval consists of the compositing period plus 10 days before and after the compositing period, thus corresponding to 21 days for the compositing periods of 1 day. Such enlargement was found to be necessary to ensure statistical values ( $\mu$  and  $\sigma$ ) were based on a sufficient amount of data. Based on these  $\mu$  and  $\sigma$  values, the three following thresholds  $\tau_1$ ,  $\tau_2$  and  $\tau_3$  have been defined:

$$\tau_1 = \frac{\sigma}{\mu}$$

$$\tau_2 = \mu + \sigma$$

$$\tau_3 = 1.35 \mu \quad \text{eq. 3-6}$$

The threshold  $\tau_3$  has been inferred from investigations about BRDF measurements in the NIR region (Schoenermark et al, 2004) achieved in the Fire\_cci/LC\_cci project, in which a "variability" of the SDR measurements between 5 to 31% was found. The threshold value was defined using the maximum variability (i.e. 31%) plus an additional safety factor. The following additional threshold has been assessed for an improvement of the efficiency of the temporal filtering:

$$\tau_4 = \rho_{band}^{MAX_{NDVI}} + 2\sigma \text{ e.g. band} = 8 \text{ (MERIS)} \quad \text{eq. 3-7}$$

A pixel would be now flagged as cloud (i.e. not clear land) if it satisfies the following conditions:

$$\tau_1 > 0.075 \text{ (MERIS)}$$

$$\rho_{band} > MIN(\tau_2, \tau_3, \tau_4) \quad \text{eq. 3-8}$$

Accordingly, the number of clear land observations in the L3 products are a combined function of the composite period but also of the temporal filter efficiency. The temporal filter efficiency depends on three main factors: (i) the length of the filter interval, (ii) the quality of IdePix results and (iii) the pixel seasonality.

<sup>7</sup> The algorithm of the clear land feature does not take into account the uncertainty.

The length of the filter interval (first factor) is related to the statistic values computation: a longer filter interval will allow more robust mean and standard deviation values ( $\mu$  and  $\sigma$ ) and hence, a higher efficiency of the filter. The IdePix performance (second factor) is also important since it will influence the proportions of correct and misclassified clear land pixels in the set of clear land pixels to reclassify through the temporal filter. If the fraction of misclassified clear land pixel is high, the corresponding SDRs lead to an increasing of the standard deviation of the calculated threshold respective and prevent an effective filtering. Finally, the pixels seasonality (third factor) also plays a role in decreasing the robustness of the mean value ( $\mu$ ).

### 3.3.6. Temporal sample aggregation

The temporal sample aggregations is, for a given pixel in a given aggregation grid cell (a spatial tile), a selection of a best observation over all input data, providing best pixel values of SDR and SDR uncertainties, and a status flag. Table 6 summarizes the types of final status flag and the following pseudo-code ( eq. 3-5) describes the temporal sample aggregation. It is worth noting that the selection process of the best pixels does not include a BRDF correction part.

**Table 6: Final status flag**

| FLAG NAME           | DESCRIPTION  |
|---------------------|--|
| CURRENT_PIXEL_STATE | final pixel classification after selection (one of the following flags)  |
| CLEAR_LAND          | pixel was classified as land   |
| CLEAR_WATER         | pixel was classified as water  |
| CLEAR_SNOW_ICE      | pixel was classified as snow/ice   |
| CLOUD               | pixel was classified as cloud or pixel was classified as 'temporal' cloud (a posteriori cloud check within the aggregation scheme) |
| CLOUD_SHADOW        | pixel was classified as cloud shadow   |
| INVALID             | pixel was classified as invalid or cosmetic <sup>8</sup>   |


- pixel classification after aggregation (X= LAND, CLOUD etc.)

*STATUS\_X*

- surfaces reflectances for N wavelengths of given sensor

$$\begin{aligned}
 \text{for } j = 1 \dots N_\lambda \text{ and } N_{obs} &:= N_{obs,STATUS_X} S_{agg} \\
 &:= SDR_{MIN}(SDR(MERIS\_BAND\_14(j;N_{obs}))
 \end{aligned}$$

<sup>8</sup> A pixel is classified as invalid, if the pixel observation is marked as erroneous by the L1b flag or the internal Fire\_cci/LC\_cci QA or the pixel values cannot be processed by the pre-processing chain, e.g. the sun observation geometry is outside the valid range for the aerosol retrieval.

|   |                                    |  |   |
|---|------------------------------------|--|---|
|  | <b>Fire_cci</b>                    |  | Ref.: Fire_cci_D2.1.1_YR1_ATBD-MERIS_v1.1 |
|   | <b>Algorithm Theoretical Basis</b> |  | Issue 1.1                                 |
|   | <b>Document – MERIS</b>            |  | Date 11/11/2016                           |
|   |                                    |  | Page 27                                   |

- NDVI<sup>9</sup>

$$\begin{aligned}
 & \text{for } j = 1 \dots N_\lambda \text{ and } N_{obs} := N_{obs,STATUS_X} \quad NDVI \\
 & \qquad \qquad \qquad := NDVI_{MIN(SDR(MERIS\_BAND\_14(j;N_{obs})))}
 \end{aligned}$$

- uncertainty of surfaces reflectances for N wavelengths of given sensor

$$\begin{aligned}
 & \text{for } j = 1 \dots N_\lambda \text{ and } N_{obs} := N_{obs,STATUS_X} \quad \Delta S_{agg} \\
 & \qquad \qquad \qquad := \Delta SDR_{MIN(SDR(MERIS\_BAND\_14(j;N_{obs})))}
 \end{aligned}$$

eq. 3-9

### 3.3.7. L3-Processing

The processing steps to retrieve the final Level 3 products from an input set of single satellite observations (i.e., SDR and pixel classification data as derived in the previous sections) are (i) the reprojection of the input products onto a Plate Carrée grid, (ii) the aggregation of the single satellite observations for given binning cells (tiles), and (iii) the mosaicking of the binning cells to a Level 3 product of 10x10 degrees with the aggregation results.

#### 3.3.7.1. Plate-Carrée projection

The plate carrée projection or geographic projection or equirectangular projection, is a very simple map projection that has been in use since the earliest days of spherical cartography. The name is from the French for "flat and square". It is a special case of the equidistant cylindrical projection in which the horizontal coordinate is the longitude and the vertical coordinate is the latitude.

The spherical earth can only be mapped onto a developable surface by allowing distortion, so certain geometric properties on the sphere are not preserved. The Plate Carrée projection is a cylindrical projection but unlike the Mercator projection, the entire sphere, including the poles can be represented on a finite sized map. The projection is not a conformal map so angles are not preserved.

Because of the distortions introduced by this projection, it has little use in navigation or cadastral mapping and finds its main use in thematic mapping. It has also become a de-facto standard for computer applications that process global maps, because a given coordinate is very easily identifiable in an image file.

The following equations describe the mapping of geographic coordinates in terms of latitude  $\varphi$  and longitude  $\lambda$  onto the x and y coordinates of a point on the map. From its latitude  $\varphi$  and longitude  $\lambda$  (with  $\varphi_0$  and  $\lambda_0$  being the latitude and longitude in the centre of map) and k being an appropriate scale factor at the equator:

$$x = k(\lambda - \lambda_0), y = k(\varphi - \varphi_0) \qquad \text{eq. 3.10}$$

For the Fire\_cci products, the geoid WGS84 is used.

<sup>9</sup> Uncertainty has not been considered in the generation of NDVI values; no uncertainty value for NDVI is provided.

### 3.3.7.2. Resampling

If a product is projected it comes up that the pixel centres of the target product generally do not correspond to the centres of the pixels of the input product. Resampling entails the process of determination and interpolation of pixels in the source product for computation of the pixel values in the target product. The effects of resampling will especially be visible if the pixels in the target product are larger than the source pixels. The following three different resampling methods for this computation have been assessed.

- Nearest Neighbour
- Bilinear Interpolation
- Cubic Convolution


However, the nearest neighbour method has been selected as resampling method for the projection because of its preservation of the original physical values.

### 3.3.7.3. Generation of mosaics

As final step, all grid cells (tiles) which were part of one or more input products for the aggregation and which were processed as described above are merged into a single Level 3 result product. Table 7 summarizes the bands, which are included in the final L3 pre-processing products for MERIS. No BRDF correction module is currently applied in the pre-processing chain.

**Table 7: Variables used in Level 3 mosaicking for MERIS**

| <b>Parameter</b>  | <b>Description</b>  |
|---|---|
| SR of band xsensor;<br>xMERIS = 1 ... 10,12 ... 14            | surface reflectance of band xsensor;<br>xMERIS = 1 ... 10,12 ... 14                         |
| $\epsilon$ SR of band xsensor;<br>xMERIS = 1 ... 10,12 ... 14 | uncertainties of the surface reflectance of band<br>xsensor;<br>xMERIS = 1 ... 10,12 ... 14 |
| Ndvi  | NDVI  |
| Status  | current pixel status classified by IdePix, clear land<br>filter and temporal filter         |
| SZA   | sun zenith angle  |
| VZA   | view zenith angle   |
| SAA   | sun azimuth angle   |
| VAA   | view azimuth angle  |

|   |  |  |       |                                     |      |
|---|--|--|-------|-------------------------------------|------|
|  | <b>Fire_cci</b><br><b>Algorithm Theoretical Basis</b><br><b>Document – MERIS</b> |  | Ref.: | Fire_cci_D2.1.1_YR1_ATBD-MERIS_v1.1 |      |
|   |  |  | Issue | 1.1                                 | Date |
|   |  |  |       |                                     | Page |

## 4. BA Algorithm description

### 4.1. General scheme

An hybrid approach was chosen to implement the MERIS BA algorithm. Therefore, active fire detection and post fire reflectance information were combined. This implementation makes profit of the advantages of both techniques, i.e. the more sensitive thermal characterisation of active fires and the more permanent reflectance changes of burned patches. Active fire detections are used to identify burned pixels or to select polygons if an object based classification has been used. This approach has been followed by several authors (Fraser and Li 2002; Fraser et al. 2000; Giglio et al. 2009; Gong et al. 2006; Pu et al. 2007; Roy et al. 1999) obtaining good results.

After literature review and study of the pre-processed MERIS data a general scheme on the initial algorithm configuration was defined. Three main lines were drawn:

- *Type of algorithm*: it was decided that the hybrid algorithm would be based on a two-phase approach (seed and growing phases). It was concluded from the literature review that this configuration would give better results than other implementations, as it would be more flexible to address the spatial heterogeneity of BA conditions in different regions.
- *Type of BA identification*: the basis to perform BA detections would be the creation of a series of composites based on NIR and spectral indices to identify the burns.
- *Auxiliary data*: MERIS does not provide information in some bands that are useful for burned area detection, and therefore the use of auxiliary information was already foreseen. A study by Hantson et al. (2013) showed that the MODIS 14 product (corresponding to hotspots/active fires) has a tendency towards omission, having low commission error rates. The low commission reported made its use interesting in the MERIS algorithm for the seed phase, since the aim is to avoid commission errors at this stage of the retrieval. The behaviour of the product in different regions was also identified. Therefore this was the product selected to identify the active fires. Other products such as the World Fire Atlas, VIIRS active fires or the SLSTR fire product could be used in a similar way to feed the BA algorithm. A fuel mask, based on the LC\_cci product, was used to mask out non-burnable areas.

The general scheme of the algorithm is shown in Figure 5. MERIS input data are used to build a series of spectral indices. This information is combined with the auxiliary data to obtain monthly and annual composites. These composites are the basis to perform the seed identification phase. Once the seeds are retrieved the growing phase of the algorithm is computed on the individual images to obtain the BA maps.

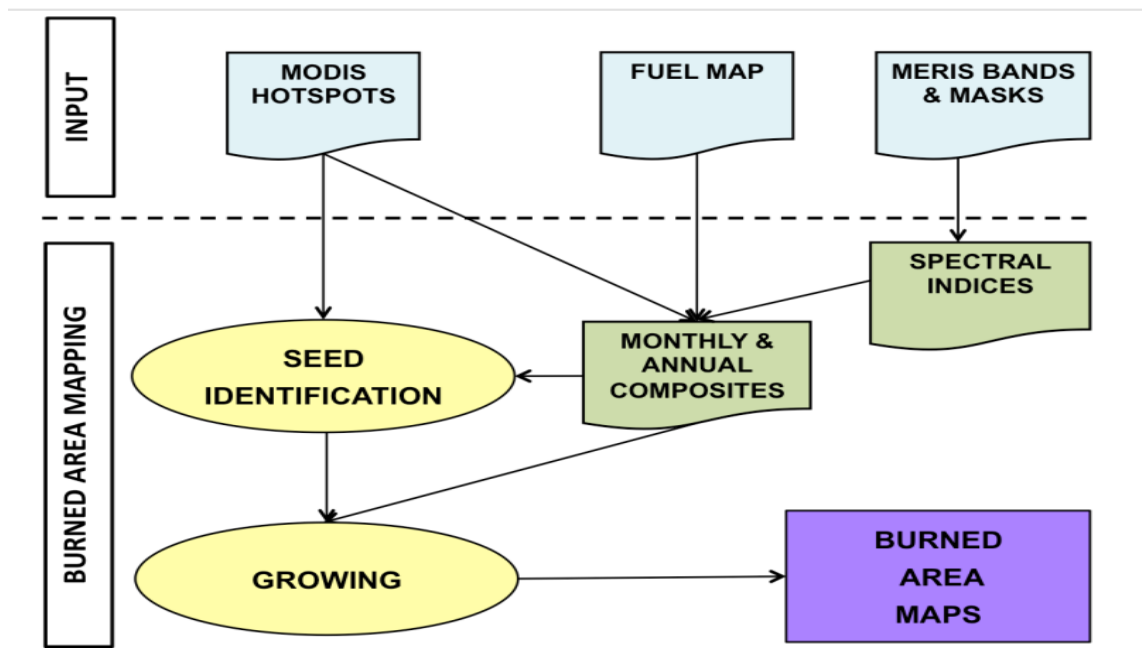


Figure 5: Algorithm main scheme definition.


## 4.2. Input data

The input data to the BA algorithm are the MERIS pre-processed reflectances tiles of 10x10 degrees obtained by processing chain explained in section 3, along with the auxiliary data (active fires and fuel mask).

The active fires or hotspots (HS) MOD14 product is generated by combining the information from the medium infra-red (MIR) and thermal infra-red (TIR) bands of the MODIS sensor using a contextual algorithm. On a first step fixed thresholds are applied to the MIR and TIR channels and then false detections are excluded by analysing the brightness temperature in neighbouring pixels (Giglio et al. 2003). Information available from MODIS in both TERRA and AQUA satellites (10.30 and 13.30 Equatorial cross time respectively) was used. The product was downloaded from the Fire Information for Resource Management System (FIRMS) (Davies et al. 2009). The product reports fires that are burning at the time of the satellite overpass at 1km resolution. This product has been used in other global BA algorithms (Giglio et al. 2009).

A fuel mask was introduced as auxiliary data into the algorithm for two reasons. Firstly, it improves processing time of the algorithm since pixels that are already masked as not burnable will not be processed. Secondly, it avoids commission errors in areas that are not burnable, i.e. have no fuels, but that for different reasons could be mapped as burned by the algorithm (dark soils, shadows).

The fuel mask is a binary mask with two classes: burnable/not burnable. It was derived from the Land Cover CCI version 1.6.1 product (<http://www.esa-landcover-cci.org> last access 29th July 2016), by converting all vegetation classes into the burnable class, whereas urban areas, deserts and water were considered non-burnable class. Two maps were derived covering the different epochs defined in the Land Cover CCI. The fuel

|   |  |  |       |                                     |      |            |
|---|--|--|-------|-------------------------------------|------|------------|
|  | <b>Fire_cci</b><br><b>Algorithm Theoretical Basis</b><br><b>Document – MERIS</b> |  | Ref.: | Fire_cci_D2.1.1_YR1_ATBD-MERIS_v1.1 |      |            |
|   |  |  | Issue | 1.1                                 | Date | 11/11/2016 |
|   |  |  |       |                                     | Page | 31         |

map for 2000 covers the period between 2003 and 2007 and the fuel map for 2005 covers the period from 2008 onwards.

### 4.3. Bands and indices selection

MERIS has 15 bands covering the VIS to NIR electromagnetic region of the spectrum. Eight of these bands are in the visible region, four in the red-edge and three in the NIR. The NIR region has been identified in several studies as being the most suitable region of the spectrum (together with the SWIR) to detect BA. NIR and the Global Environmental Monitoring Index (GEMI) have been extensively used for burned area mapping in different ecosystems (Barbosa et al, 1999 in Africa; Pereira, 1999 in a comparative study with AVHRR data; Chuvieco et al, 2002 in Mediterranean areas; Martin et al., 2005 in the Mediterranean; Chuvieco et al., 2008 in Boreal forest). A study performed by Oliva et al. (2010) showed the adequacy of bands 8 and 10 to map burned area. Therefore those were the bands selected to perform the BA detections. Furthermore, the GEMI index was specifically designed to diminish the influence of atmospheric and soil effects (Pinty and Verstraete 1992). The GEMI expression is:

$$GEMI = \eta * (1 - 0,25\eta) - \frac{\rho_R - 0,125}{1 - \rho_R} \quad \text{eq. 4.1}$$

Where

$$\eta = \frac{2 * (\rho_{IR}^2 - \rho_R^2) + (1,5 * \rho_{IR}) + (0,5 * \rho_R)}{\rho_{IR} + \rho_R + 0,5} \quad \text{eq. 4.2}$$

Being  $\rho_R$  and  $\rho_{IR}$  the reflectivity in the red and infra-red bands, respectively.

GEMI and NIR should show a significant decrease when a fire occurs. This is commonly the case, as shown in Figure 6, when the fire occurs on day 280 (according to the HS product, grey arrow). Changes in the expected behaviour may be caused by other factors, such as clouds, shadows, haze, snow melting or floods not detected correctly and masked by the pre-processor, as illustrated in Figure 7. In this case the HS labels the fire on day 263 (grey arrow) but there is a significant NIR and GEMI decrease prior to this event, on day 228 (blue arrow).

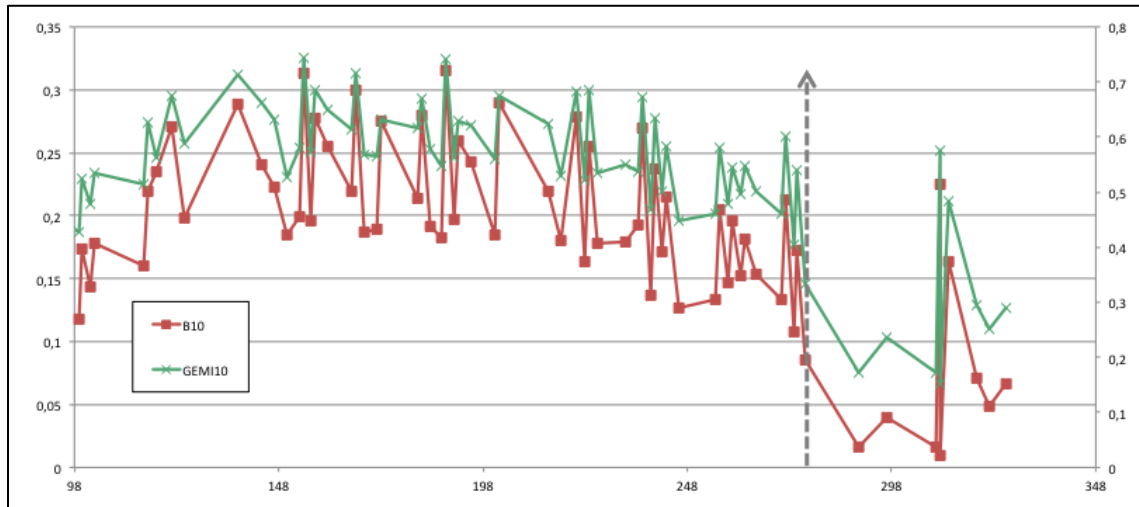


Figure 6: Temporal evolution of NIR and GEMI for a pixel in Portugal.

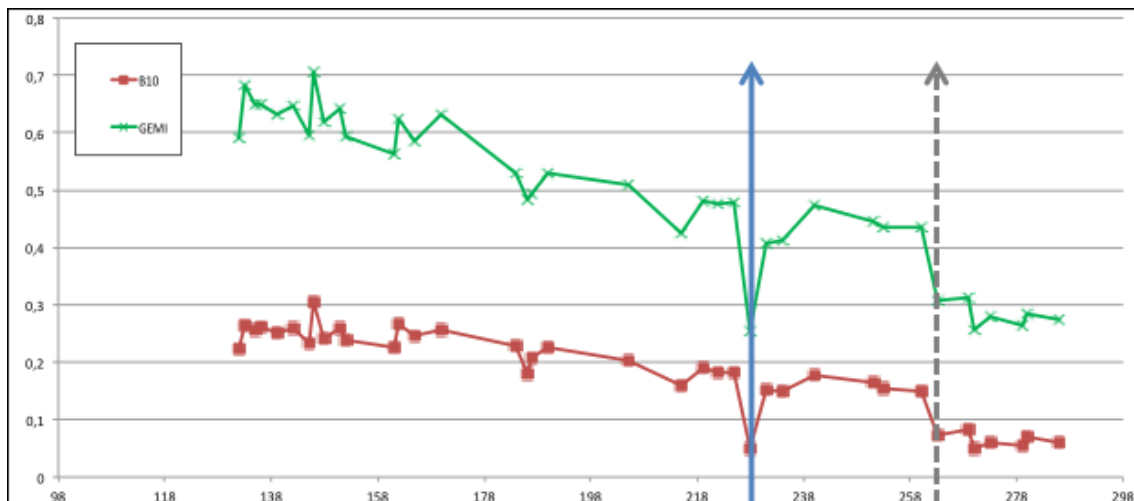


Figure 7: Temporal evolution of NIR and GEMI for a pixel in Portugal.

#### 4.4. Monthly and annual composites

Monthly composites were built in the MERIS BA algorithm to ensure spatial and temporal consistency of the burned pixel detections. Several compositing techniques mostly based on spectral criteria have been proposed in the literature (Chuvienco et al., 2005). In this case, we have used the dates of the HS as the compositing criterion, as it was expected that they would tend to select the closest pixels to the dates of burning. For doing so, we first built Thiessen polygons (Brassel and Reif 1979) around each HS. The resulting Thiessen matrix assigned to each pixel the date of the closest HS. Afterwards, we built a NIR post-fire composite guided from this Thiessen matrix, relying therefore on the high temporal accuracy of HS (Boschetti et al, 2010).

It is well known that HS do not provide a full description of fire-affected areas, as satellite sensors only detect those fires that are active when the satellite overpasses the fires. However, the high thermal contrast between burning and background pixels and the sensitivity of MODIS thermal channels, ensures a high confidence in detecting





actual fires, avoiding commission errors. Hantson et al. (2013) performed an exploratory analysis of HS performance to detect burned perimeters by comparing HS with fire reference data extracted from Landsat TM/ETM+. Commission errors found were very low (<3 %) for all study sites, but omission errors (burned patches undetected) were relatively high (>25%) particularly for small BA patches. The HS were used to establish the most appropriate date for the post-fire temporal compositing. The technique of using HS for labelling fire dates has been proposed by other authors (Boschetti et al. 2010).

An example of the Thiessen HS matrix obtained for tile v10h30 (located in Northern Australia) in October 2008 is shown in Figure 8.

In order to increase the spatial consistency of the resulting composites it was decided to extend the compositing time. Composites were built for each month by selecting images from a bi-monthly time series (Figure 9). This strategy decreases the effects of low number of valid observations for cloudy regions and helps detecting fire burned areas that occurred at the end of the monthly period.

### Australia HS Thiessen matrix October 2008

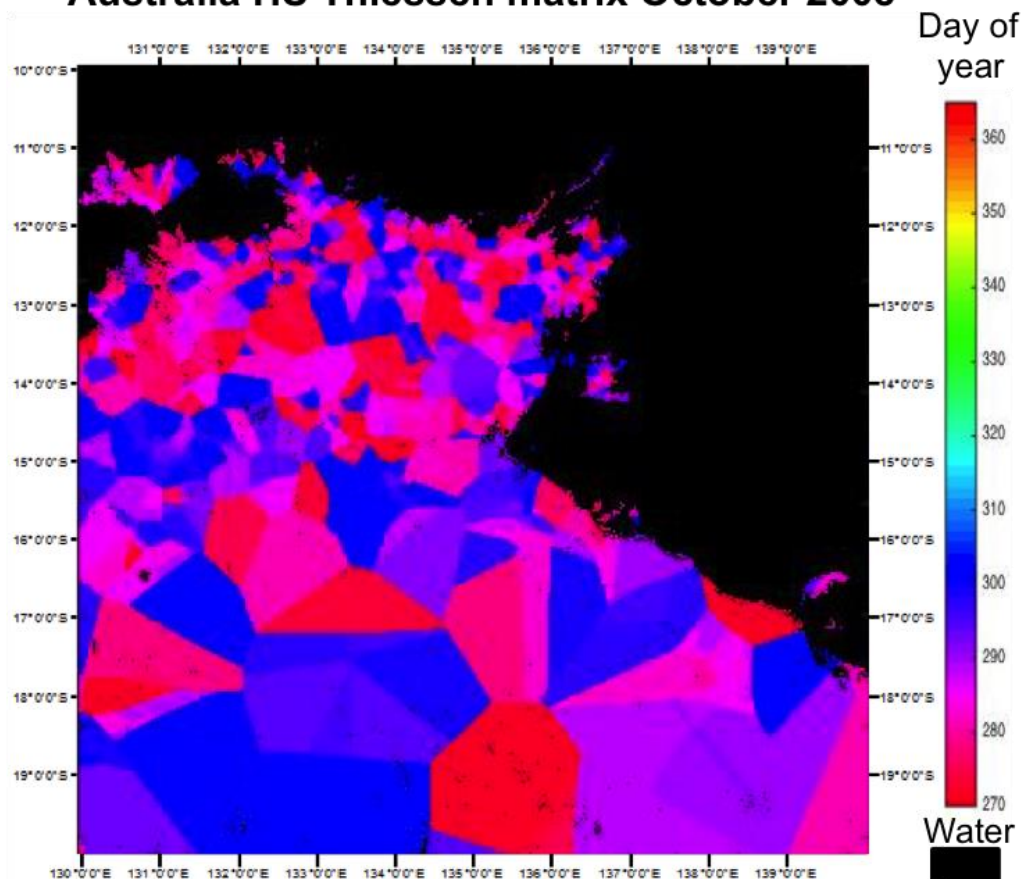
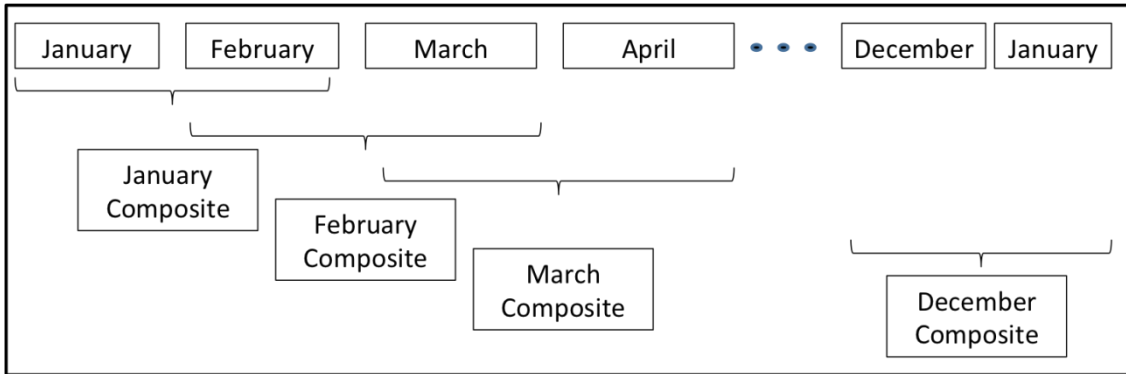
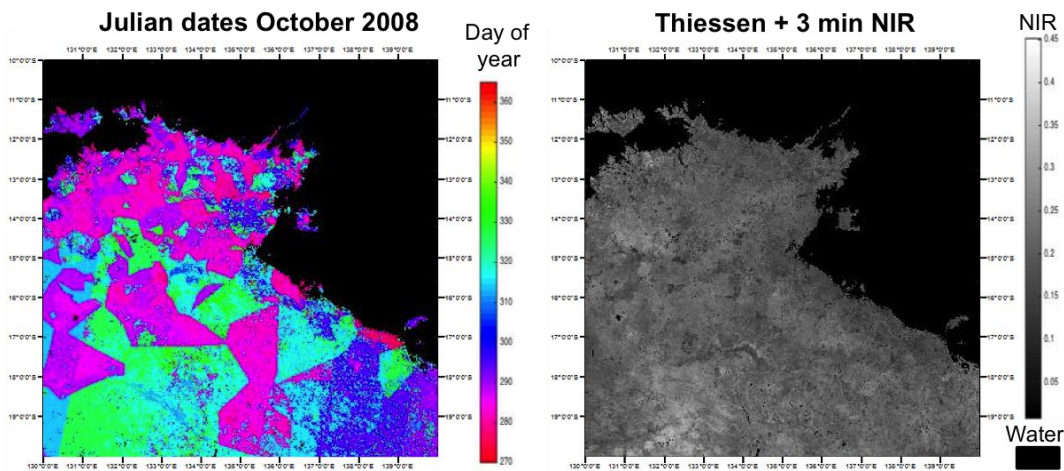


Figure 8: HS Thiessen matrix for Northern Australia in October 2008.



**Figure 9: Monthly composites generation based on MERIS information from two consecutive months.**

Low NIR values are expected in areas where char or scorched leaves are present, although they can also be caused by water or dark soils. Therefore, in case of a fire event, the NIR value should decrease, presenting significantly lower values on the days after the fire event. A minimum NIR value could therefore be found in areas that have recently burned. Considering the noise in the time series (Figure 6 and Figure 7), it was decided to identify 3 NIR minima over two months, instead of identifying a single NIR minimum value. From these minima, the one with the date after the HS and closest to the HS date was selected. If no minima were identified after the HS then the 2nd minima before the HS date was selected. This strategy would avoid potential problems not detected in the pre-processing such as cloud shadows. The 2nd NIR minima should still be representative of the fire event. An example of the NIR post fire composite and the Julian dates associated is shown in Figure 10 for the same Australian region.



**Figure 10: NIR post fire and julian dates composites for Australia in October 2008.**

In addition to the monthly post-fire composites, an annual reference composite was created for the contextual phase of the algorithm. This annual reference composite was obtained as the difference between the annual maximum GEMI value and the monthly GEMI composite. The maximum annual composite of the GEMI value should account for the maximum seasonal greenness of each pixel. The difference with the monthly GEMI indices was obtained as it was assumed that the change between the annual maximum and the post-fire value (included in the GEMI monthly composite) should be the highest for burned pixels, thus emphasising post-fire spectral changes. The GEMI

monthly composite was obtained by computing the GEMI index for the same dates used in the NIR composite previously described. An example of these is shown in Figure 11.

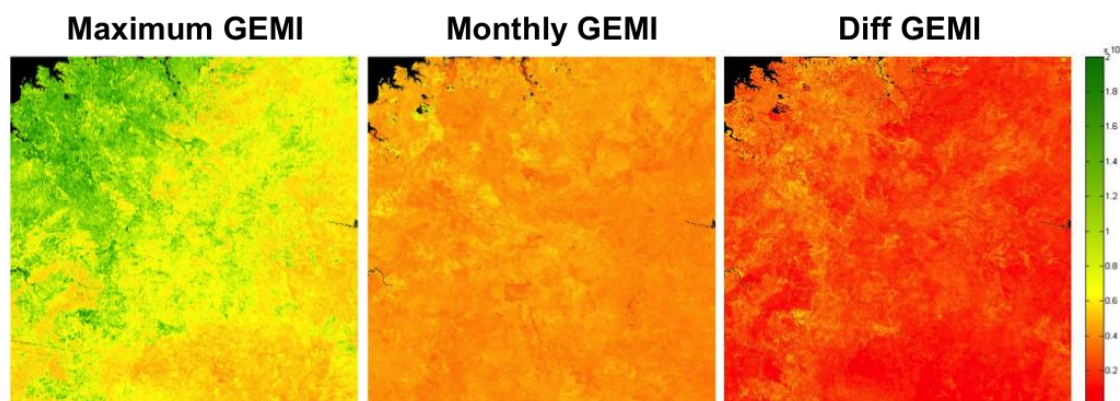


**Figure 11: Maximum annual GEMI, October 2008 GEMI and difference between them in Australia.**

The steps to build the monthly composites are illustrated in Figure 12. Final composites (NIR, Julian dates and DiffGEMI) are highlighted in green. The first two are used in the seed and growing phases of the algorithm, while DiffGEMI is used only in the growing phase of the algorithm.

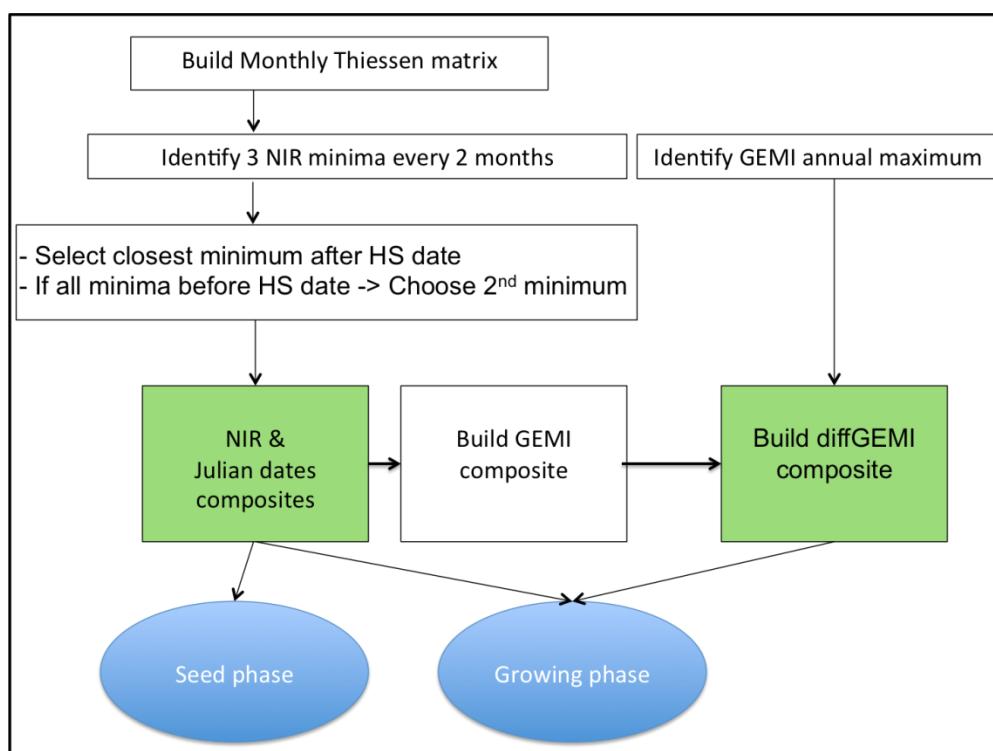


**Figure 12: Steps to build the final composites.**

#### 4.5. Seed phase

The seed concept is based on the identification of pixels where there is a high confidence on those pixels having burned. The bottom line is to have little omission in this phase (detection of maximum number of perimeters), while keeping a low



commission rate. In the MERIS BA algorithm, the starting point was the definition of two different classes (burned and unburned). The purpose was to maximise the distance between these two classes to identify a threshold that could reasonably separate them. In addition, these thresholds should be dynamically (spatially and temporally) adapted to the fire characteristics of each region and season, as fire characteristics change both spatially and temporally.

For doing so, a series of rules were needed to identify the set of pixels that would help defining the burned and unburned classes. The approach was based on the use of HS to identify potential burned pixels, and by contrast the unburned ones. Those pixels that fulfilled a set of requirements were used to build the cumulative distribution functions (CDFs), used to represent the burned and unburned classes. From these functions, a threshold was established to identify seed pixels. Those threshold values were chosen to minimise the confusion between the two classes and were computed for each tile of the input MERIS reflectances ( $10^{\circ} \times 10^{\circ}$  or  $3600 \times 3600$  pixels at MERIS FR). Figure 13 illustrates the distributions and CDFs concept. On the left side two normal distributions are plotted. The top left one shows the case where the two distributions are closer, and therefore more confusion between the classes existed, since more values were shared between them. This translated also into closer CDFs (top right). On the bottom, the opposite case is represented, with a much clearer separation between classes, i.e. the distributions shared fewer values and therefore the confusion was lower.

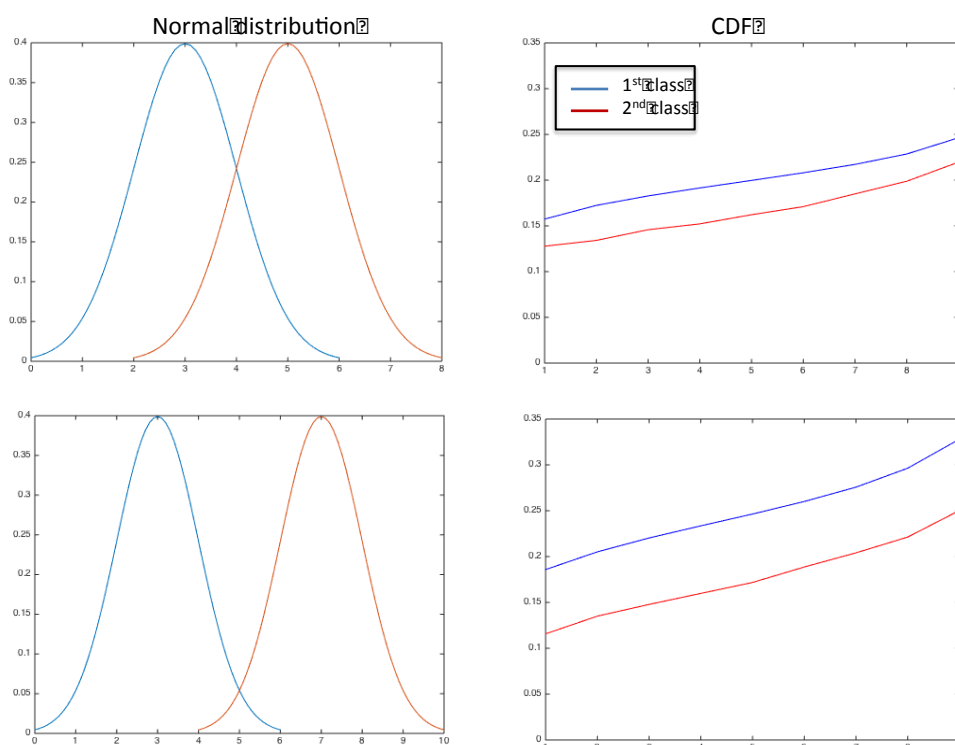


**Figure 13: Normal distributions and CDFs showing the poor and better separation between classes.**

The  $10^{\circ} \times 10^{\circ}$  tiles that were the output of pre-processing chain were used to obtain the statistics and CDF values. It was decided to keep them as input to the algorithm and to obtain the CDFs as this division offered a good balance between regional diversity and processing time.

#### 4.5.1. Threshold selection

A threshold value was needed to identify which pixels would be classified as seeds. This threshold was defined on a regional basis and in monthly time periods. It was selected from the immediate lower decile of the burned curve that corresponds to the first decile of the unburned curve.

The conditions to define the burned and unburned CDFs used to select the threshold are:

- *Unburned CDF*: Unburned pixels were extracted from areas without a single HS in the vicinity and that had not previously burned. The area was defined by a matrix size of 64x64 MERIS pixels. Values bigger than 64x64 could give problems in areas with very high fire activity, or in areas where the proportion of land in the tile is low (water or non-burnable pixels).
- *Burned CDF*: Minimum NIR with median decrease in NIR reflectance. The spatial resolution is different between a HS (1km) and a MERIS pixel (300m). Therefore, 9 MERIS pixels fall within a single HS. It was decided to identify from the 9 MERIS pixels within the HS pixel which one had the lowest NIR value, selecting this one as more representative of the burning. Figure 14 illustrates this concept. The 9 MERIS pixels that fall within a HS are represented, with the centre of the HS being the red dot. The minimum NIR pixel is highlighted in blue. For those minimum NIR pixels identified, the median of the NIR reflectance for 5 daily values before and after the HS date was computed. If the pre median value was higher than the post, the pixel was identified as Potential active fire (PAF) and used to build the burned CDF.

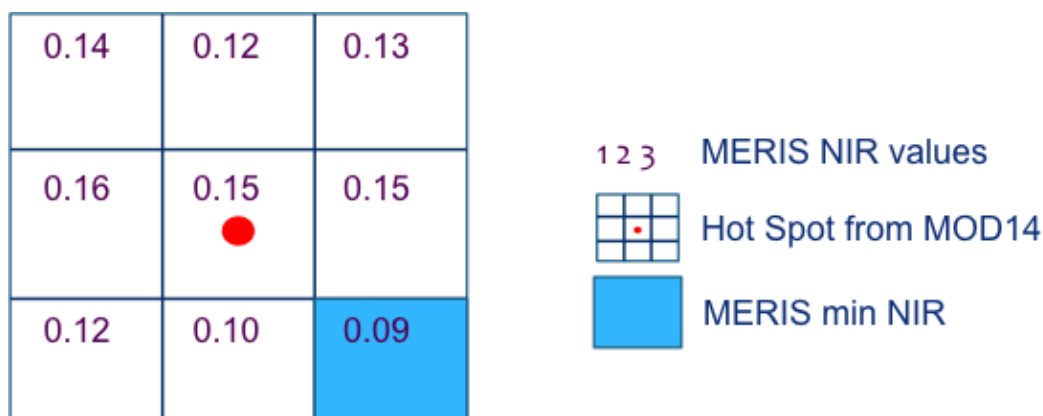


Figure 14: Selection of PAF within a MERIS 3x3 window with a HS.

#### 4.5.2. Seed identification

Once the threshold was identified, a set of conditions needed to be verified to classify a pixel as seed. They are as follows:

- *Ratio HS/PAF*: the number of pixels resultant from the filtering of HS with the median technique provides an idea on the number of commission errors that exist in that area for the MOD14 product. Therefore, this information could also be used to define more or less restrictive conditions to classify the pixels as seed. The ratio between HS and PAFs was computed. If the ratio was smaller than 2, a single PAF

per matrix was required. If this relation was bigger than 2, the number of PAFs per matrix required to classify a pixel as burned increased to 2.

- NIR value lower than the threshold identified from the CDF (immediate lower decile of the burned curve that corresponds to the first decile of the unburned curve).
- Maximum distance to a PAF should be below a certain value. The seed should have at least one PAF within a matrix of 9x9 around the pixel analysed. In case the ratio between the seeds and the HS was bigger than 12 two PAFs were needed in the 9x9 matrix to be considered a seed. This restriction was applied to further limit commission errors in the seed phase.

Figure 15 summarizes the main steps to be performed in the seed phase of the BA MERIS algorithm.

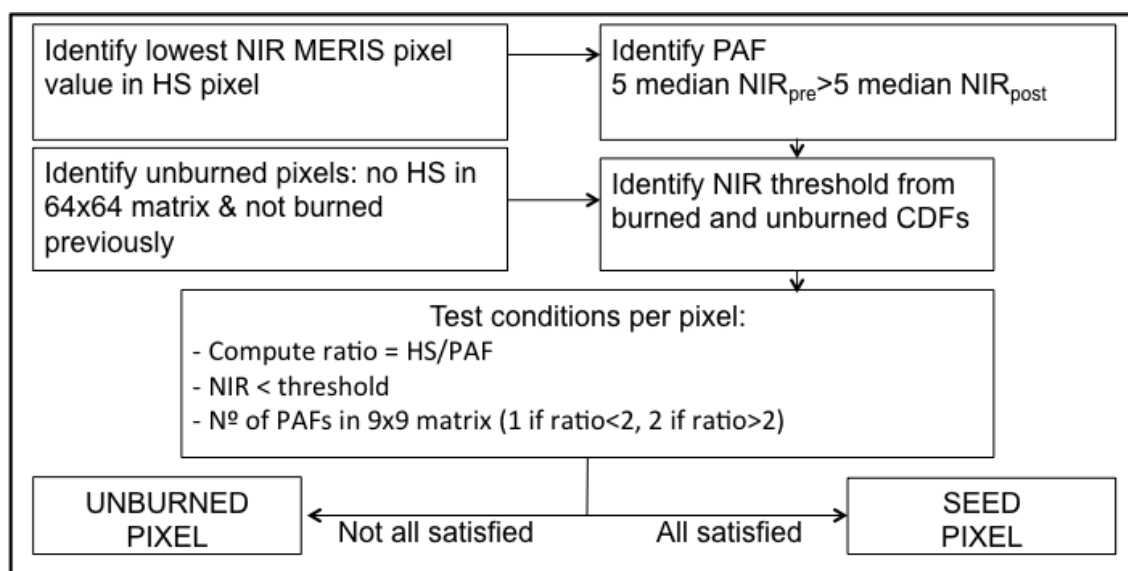


**Figure 15: Main steps to identify seed pixels.**

#### 4.6. Growing phase

In the growing phase of the algorithm the aim was to improve the delimitation of BA patches applying contextual algorithms to the seed pixels. Those pixels located in the neighbourhood of the seed pixels were candidates to extend the BA area if they fulfilled additional requirements (spectral similarity with the seed pixels and NIR values below a growing threshold). In the MERIS BA algorithm version 4.1 individual images were used to extend the BA. Burned and unburned CDFs were re-computed for each individual image. In the growing phase the unburned CDF was computed following the same procedure of the seed phase, whereas the burned CDF was computed with the seed pixels identified for the day that was being analysed. The growing threshold was identified again as the immediate lower decile of the burned curve that corresponds to the first decile of the unburned curve. In other words, the NIR value was a bit higher than for the seed phase, as the growing phase is less restrictive.

Three conditions needed to be satisfied by each pixel to be classified as burned:


- NIR value lower than the growing phase threshold.
- The diffGEMI annual composite had to verify a decreasing threshold between seed and neighbour pixels. Pixels were classified as burned if the neighbours to a seed pixel had higher values than the threshold. The threshold was defined from the diffGEMI value found in the seed pixel multiplied by 0.9.
- The difference in NIR values from the image under analysis (in month N) and the NIR composite in month N-1 is a negative value. This ensures a decrease in NIR reflectance.

Figure 16 illustrates the growing phase procedure.

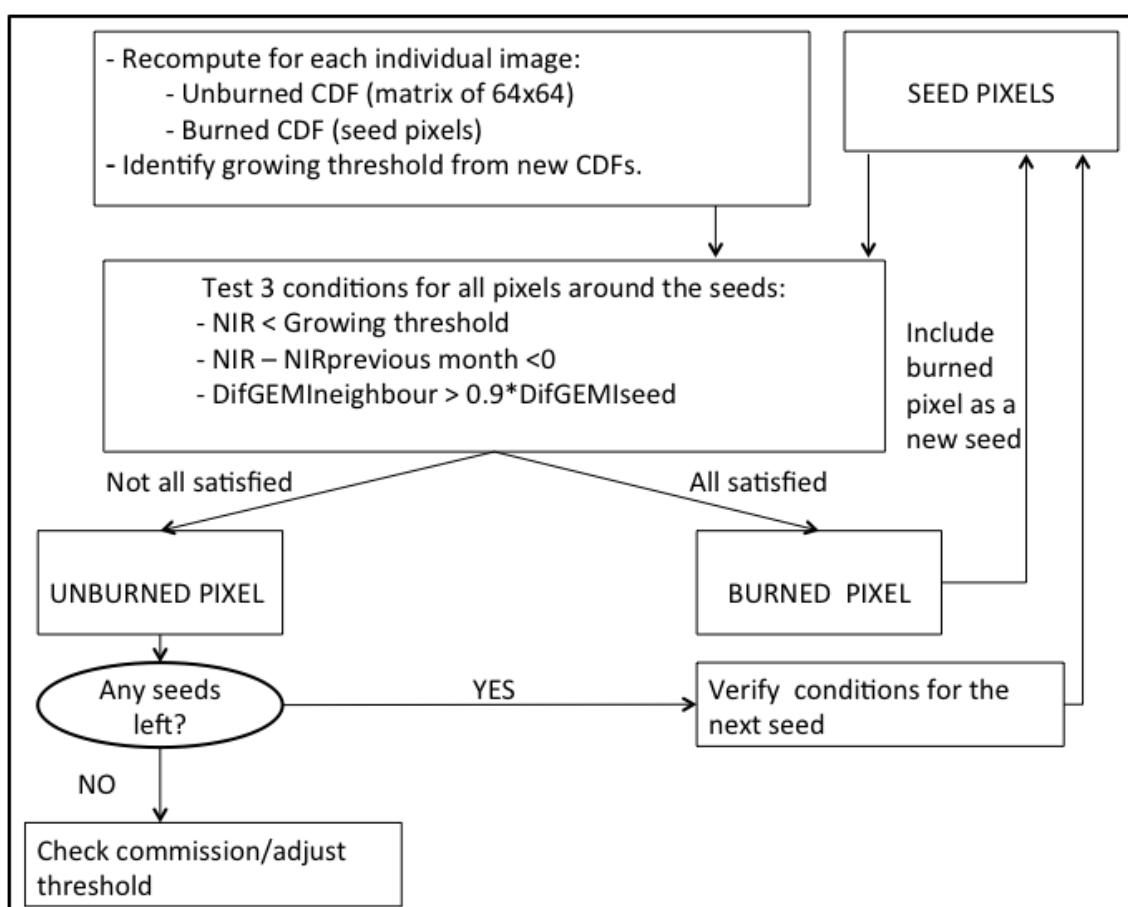


**Figure 16: Growing phase main steps.**

A final test was applied to avoid large commission errors in a few areas with dark covers, where the region growing process might not perform properly (specific regions of Australia, China and India, for instance). In this case, large polygons were filtered out when the number of burned pixels exceeded largely the number of hotspots or seeds. Two ratios were computed. First the ratio between the BA found per image and the seeds in the image. If this ratio was bigger than 200 a more restrictive threshold (growing threshold decile - 2) was applied. A second ratio between the BA per month and the number of HS per month was also obtained. In case this value was bigger than 100 a more restrictive threshold (growing threshold decile - 2) was applied to the growing phase.

|   |  |       |                                     |      |            |    |
|---|--|-------|-------------------------------------|------|------------|----|
|  | <b>Fire_cci</b><br><b>Algorithm Theoretical Basis</b><br><b>Document – MERIS</b> | Ref.: | Fire_cci_D2.1.1_YR1_ATBD-MERIS_v1.1 |      |            |    |
|   |  | Issue | 1.1                                 | Date | 11/11/2016 |    |
|   |  |       |                                     |      | Page       | 40 |

It is important to note that version 4.1 of the algorithm considers the possibility of double burns, i.e. pixels that burn twice in the same year. The minimum time gap between these two burns is 5 months. Therefore pixels detected as burned within a 5 months' time span would not be considered as burned twice.

#### 4.7. MERIS BA algorithm auxiliary output layers

In addition to the burned area detection the MERIS BA algorithm computes another 5 layers of information. These are required by the formatting tool to generate the final BA product that is delivered to the users. The five layers are:

1. Confidence level: it was obtained based on Bayes' theorem:

$$P(B/ NIR) = (100 * P(NIR/ B) * P_B) / P(NIR/ B) * P_B + P(NIR/ U) * P_U$$

Where:

- $P(B/NIR)$  = probability of having burned given the fact that it has a particular NIR value.
- $P(NIR/B)$  = probability of observing a certain value of NIR knowing that it has burned.
- $P(NIR/U)$  = probability of observing a certain NIR value knowing that it has not burned.
- $P_B = 0.5$  = a priori probability of burning
- $P_U = 0.5$  = a priori probability of not burning

The confidence level is computed only for the burned pixels.

2. Valid\_before: last valid observation before the date of burn within a 30 days range.


This information is computed only for the burned pixels.

3. Number of valid observations for the month under evaluation.

4. Total number of observations for the month under evaluation.

5. Number of cloudy observations for the month under evaluation.



|   |  |  |       |                                     |      |            |
|---|--|--|-------|-------------------------------------|------|------------|
|  | <b>Fire_cci</b><br><b>Algorithm Theoretical Basis</b><br><b>Document – MERIS</b> |  | Ref.: | Fire_cci_D2.1.1_YR1_ATBD-MERIS_v1.1 |      |            |
|   |  |  | Issue | 1.1                                 | Date | 11/11/2016 |
|   |  |  |       |                                     | Page | 41         |

## 5. Formatting tool

This piece of software was designed to obtain the final pixel and grid products following the specifications of the PSD (Chuvienco et al., 2016b).

### 5.1. Pixel product

The pixel products are stitched products which consist of the result of the BA algorithm described in the previous section. They keep the resolution, so the pixel values are directly copied.

In the PSD, there have been defined 6 zones, for which the pixel products are created: North and South America, Europe, Africa, Asia, and Australia. Each pixel product consists of three image layers: JD (the day of the year on which the fire has occurred), CL (the level of confidence of the observation), and LC (the land cover class, according to the PSD).

In the following sections, it is explained how these three layers are derived from the BA algorithm result.

#### 5.1.1. JD

The JD layer is nearly simply copied over; the one exception occurs when the LC class is an invalid LC class in Fire\_cci, in which case the pixel is set to non-burned.

With BA the result of the burned area algorithm, and LC the land cover information:

```


for each pixel p in the output product, do:
    if LC is invalid LC_CLASS:
        set JD(p) = 0
    else:
        set JD(p) = BA

```

#### 5.1.2. CL

The CL layer is nearly simply copied over as well. If the LC class is an invalid LC class in Fire\_cci, the confidence level is set to 0. Otherwise, the confidence level is copied and scaled.

With BA the result of the burned area algorithm, CL the confidence level output by the burned area algorithm, and LC the land cover information:

|   |  |  |       |                                     |      |            |
|---|--|--|-------|-------------------------------------|------|------------|
|  | <b>Fire_cci</b><br><b>Algorithm Theoretical Basis</b><br><b>Document – MERIS</b> |  | Ref.: | Fire_cci_D2.1.1_YR1_ATBD-MERIS_v1.1 |      |            |
|   |  |  | Issue | 1.1                                 | Date | 11/11/2016 |
|   |  |  |       |                                     | Page | 42         |

for each pixel  $p$  in the output product, do:

```

if BA == 999:
    set CL(p) = 999
else if LC is invalid LC_CLASS:
    set CL(p) = 0
else:
    set CL(p) = CL / 100

```

### 5.1.3. LC

The CL layer is copied over from the LC data, but only where BA information is available.

With BA the result of the burned area algorithm and LC the land cover information:

for each pixel  $p$  in the output product, do:

```

if BA == 999:
    set LC(p) = 999
else if BA == 0:
    set LC(p) = 0
else:
    set LC(p) = LC

```

## 5.2. Grid product


The grid products are global products which aggregate the result of the BA algorithm described in the previous section. They are mapped onto a  $0.25^\circ$ /pixel grid. Hence, the pixels in the result of the BA algorithm cannot simply be copied, but need some kind of aggregation.

This aggregation is reflected in the first layer of the grid products, which is the sum of BA. This does not provide the binary information burned/unburned, but rather the amount of burned area. The other layers are the standard error of the burned area, the fraction of the observed area, the number of patches, and the sum of burned area of each land cover class.

In the following sections, it is explained how these layers are derived from the BA algorithm result.

### 5.2.1. Sum of BA (burned\_area)

The sum of burned area is given in  $m^2$ , and computed by identifying for each pixel in the target grid the pixels of the source grid. The grids have been chosen in such a way that for each target pixel there are  $40 \times 40$  source pixels.

|   |  |  |       |                                     |      |            |
|---|--|--|-------|-------------------------------------|------|------------|
|  | <b>Fire_cci</b><br><b>Algorithm Theoretical Basis</b><br><b>Document – MERIS</b> |  | Ref.: | Fire_cci_D2.1.1_YR1_ATBD-MERIS_v1.1 |      |            |
|   |  |  | Issue | 1.1                                 | Date | 11/11/2016 |
|   |  |  |       |                                     | Page | 43         |

```

for each pixel p in the target grid, do:
  for each source pixel ps in the source file, do:
    if ps is in valid LC class:
      burned_area(p) = burned_area (p) + area(ps)

```

### 5.2.2. Standard error (SE)

The standard error also is given in unit m<sup>2</sup>. It is computed after the burned area has been identified, on basis of the full area of each pixel and the burned area. Further description on the methodology to obtain the standard error is available in the Algorithm Theoretical Basis Document Volume III (Tansey et al. 2014).

```

for each pixel p in the target grid, do:
  ba = compute BA(p)
  area = area of p
  SE(p) = predict error(ba, area)

```

### 5.2.3. Fraction of observed area (OAF)

The fraction of observed area is given as a unitless value between 0 and 1, where a pixel value of 1 indicates that the whole area covered by the pixel has been observed, a value of 0 indicates that no source pixels of the area covered by the pixel has been observed.


```

for each pixel p in the target grid, do:
  for each source pixel ps in the source landcover file, do:
    if status of ps == 1:
      OAF_temp = OAF_temp + area(ps)
  OAF(p) = OAF_temp / area(p)

```

### 5.2.4. Number of patches (patch\_number)

The number of patches provides for each pixel the count of different patches within the pixel. A patch is a contiguous group of burned pixels. The algorithm to find the patches is a modified standard graph traversing algorithm called depth-first-search, see e.g. Wikipedia: [https://en.wikipedia.org/wiki/Depth-first\\_search](https://en.wikipedia.org/wiki/Depth-first_search).

|   |  |  |       |                                     |      |            |
|---|--|--|-------|-------------------------------------|------|------------|
|  | <b>Fire_cci</b><br><b>Algorithm Theoretical Basis</b><br><b>Document – MERIS</b> |  | Ref.: | Fire_cci_D2.1.1_YR1_ATBD-MERIS_v1.1 |      |            |
|   |  |  | Issue | 1.1                                 | Date | 11/11/2016 |
|   |  |  |       |                                     | Page | 44         |

```

for each pixel p in the target grid, do:
  for each source pixel ps, do
    run depth-first-search
    if burned pixel is encountered:
      mark pixel as burned
      increment count of patches
  patch_number(p) = count of patches

```

### 5.2.5. Sum of BA of each LC class

The sum of BA in each land cover class allows differentiating between the burns. For each LC class, it is computed as follows:


```

for each pixel p in the target grid, do:
  for each source pixel ps, do
    if ps in current LC class:
      BA(current LC class, p) = BA(current LC class, p)
+ area(ps)

```


### 5.3. Product availability

The final product is available at the CCI Data Portal, with an information link at <http://www.esa-fire-cci.org/>,


|   |                                    |  |   |            |
|---|------------------------------------|--|---|------------|
|  | <b>Fire_cci</b>                    |  | Ref.: Fire_cci_D2.1.1_YR1_ATBD-MERIS_v1.1 |            |
|   | <b>Algorithm Theoretical Basis</b> |  | Issue                                     | 1.1        |
|   | <b>Document – MERIS</b>            |  | Date                                      | 11/11/2016 |
|   |                                    |  | Page                                      | 45         |

## 6. References

- Alonso-Canas, I., & Chuvieco, E. (2015). Global Burned Area Mapping from ENVISAT-MERIS data Remote Sensing of Environment, Remote Sensing of Environment, 163, 140-152. <http://dx.doi.org/10.1016/j.rse.2015.03.011>.
- Aoki, T., Hori, M., Motoyoshi, H., et al. (2007) ADEOS-II/GLI snow/ice products — Part II: Validation results using GLI and MODIS data. Remote Sensing of Environment, 111, 274-290.
- Barbosa, P.M., Stroppiana, D., Gregoire, J.M., & Pereira, J.M.C. (1999). An assessment of vegetation fire in Africa (1981-1991): Burned areas, burned biomass, and atmospheric emissions. Global Biogeochemical Cycles, 13, 933-950
- Boschetti, L., Roy, D.P., Justice, C.O., & Giglio, L. (2010). Global assessment of the temporal reporting accuracy and precision of the MODIS burned area product. International Journal of Wildland Fire, 19, 705-709.
- Bouvet M., Ramoino F. (2010) Equalization of MERIS L1b products from the 2nd reprocessing, ESA TN TEC-EEP/2009.521/MB (available on demand at mbouvet@esa.int).
- Bourg, L., and F. Etanchaud, 2007, The AMORGOS MERIS CFI (Accurate MERIS Ortho-Rectified Geo-location Operational Software) Software User Manual & Interface Control Document, PO-ID-ACR-GS-0003.
- Bourg et al., (2011a) The AMORGOS MERIS CFI (Accurate MERIS Ortho-Rectified Geo-location Operational Software) RR Processing – Validation report (PO-RP-ACR-GS-0014; L. Bourg; ACRI-ST).
- Bourg et al., (2011b) MERIS 3rd data reprocessing Software and ADF updates, A879.NT.008.ACRI-ST, ACRI-ST.
- Brassel, K.E., & Reif, D. (1979). A procedure to generate Thiessen polygons. Geographical Analysis, 11, 289-303
- Chuvieco, E., Martín, M.P., & Palacios, A. (2002). Assessment of different spectral indices in the red-near-infrared spectral domain for burned land discrimination. International Journal of Remote Sensing, 23, 5103-5110.
- Chuvieco, E., Ventura, G., Martín, M.P., & Gomez, I. (2005). Assessment of multitemporal compositing techniques of MODIS and AVHRR images for burned land mapping. Remote Sensing of Environment, 94, 450 – 462.
- Chuvieco, E., Englefield, P., Trishchenko, A.P., & Luo, Y. (2008). Generation of long time series of burn area maps of the boreal forest from NOAA–AVHRR composite data. Remote Sensing of Environment, vol. 112, 2381-2396
- Chuvieco, E., Yue, C., Heil, A., Mouillot, F., Alonso-Canas, I., Padilla, M., Pereira, J.M., Oom, D., & Tansey, K. (2016a). A new global burned area product for climate assessment of fire impacts. Global Ecology and Biogeography, 25, 619-629.
- Chuvieco, E., A. Heil, M.L. Pettinari, A. Heil and T. Storm (2016b) ESA CCI ECV Fire Disturbance: Product Specification Report, version 6.0. Available at: <http://www.esa-fire-cci.org/documents>

|   |                                    |  |   |            |
|---|------------------------------------|--|---|------------|
|  | <b>Fire_cci</b>                    |  | Ref.: Fire_cci_D2.1.1_YR1_ATBD-MERIS_v1.1 |            |
|   | <b>Algorithm Theoretical Basis</b> |  | Issue                                     | Date       |
|   | <b>Document – MERIS</b>            |  | 1.1                                       | 11/11/2016 |
|   |                                    |  | Page                                      | 46         |

- Cox, C., and W. Munk (1954). Measurements of the roughness of the sea surface from photographs of the sun's glitter. *J. Opt. Soc. Am.*, 44, 838-850
- Davies, D., Ilavajhala, S., Wong, M., & Justice, C. (2009). Fire information for resource management system: archiving and distributing MODIS active fire data. *Geoscience and Remote Sensing, IEEE Transactions on*, 47, 72-79.
- Fell F., and J. Fischer (2001) Numerical simulation of the light field in the atmosphere-ocean system using the matrix-operator method, *Journal of Quantitative Spectroscopy & Radiative Transfer*, 69, 351-388.
- Fischer J., and H. Grassl (1984) Radiative transfer in an atmosphere-ocean system: an azimuthally dependent matrix-operator approach, *Applied Optics*, 23, 1032-1039.
- Fraser, R.H., & Li, Z. (2002). Estimating fire-related parameters in boreal forest using SPOT VEGETATION. *Remote Sensing of Environment*, 82, 95-110
- Fraser, R.H., Li, Z., & Cihlar, J. (2000). Hotspot and NDVI Differencing Synergy (HANDS): a new technique for burned area mapping over boreal forest. *Remote Sensing of Environment*, 74, 362-376
- Giglio, L., Descloitres, J., Justice, C.O., & Kaufman, Y.J. (2003). An Enhanced Contextual Fire Detection Algorithm for MODIS. *Remote Sensing of Environment*, 87, 273-282
- Giglio, L., Loboda, T., Roy, D.P., Quayle, B., & Justice, C.O. (2009). An active-fire based burned area mapping algorithm for the MODIS sensor. *Remote Sensing of Environment*, 113, 408-420
- GlobAlbedo\_ATBD/BBDRv1.0 (2010) GlobAlbedo Project: GlobAlbedo\_BBDR\_ATBD version 1.1 – only available on request.
- GlobAlbedo\_ATBDv4.12 (2013) GlobAlbedo Consortium, GlobAlbedo Algorithm Theoretical Basis Document Version 4.12, [http://www.globalbedo.org/docs/GlobAlbedo\\_Albedo\\_ATBD\\_V4.12.pdf](http://www.globalbedo.org/docs/GlobAlbedo_Albedo_ATBD_V4.12.pdf).
- GlobCover\_DJFv3.8 (2008) GlobCover 2005 project, Design Justification File, I3.8 – only available on request.
- Gong, P., Pu, R.L., Li, Z.Q., Scarborough, J., Clinton, N., & Levien, L.M. (2006). An integrated approach to wildland fire mapping of California, USA using NOAA/AVHRR data. *Photogrammetric Engineering and Remote Sensing*, 72, 139-150.
- Hantson, S., Padilla, M., Corti, D., & Chuvieco, E. (2013). Strengths and weaknesses of MODIS hotspots to characterize global fire occurrence. *Remote Sensing of Environment*, 131, 152-159.
- Hori, M., Aoki, T., Stamnes, K., Li, W. (2007) ADEOS-II/GLI snow/ice products — Part III: Retrieved results, *Remote Sensing of Environment*, 111, 291-336.
- Hu, B., Lucht, W., and Strahler, A. H. (1999) The interrelationship of atmospheric correction of reflectances and surface BRDF retrieval: a sensitivity study, *IEEE Transactions on Geoscience and Remote Sensing*, 37:724–738.
- Kaufman, Y. J. (1989) The atmospheric effect on remote sensing and its correction. In

|   |  |       |                                     |      |            |
|---|--|-------|-------------------------------------|------|------------|
|  | <b>Fire_cci</b><br><b>Algorithm Theoretical Basis</b><br><b>Document – MERIS</b> | Ref.: | Fire_cci_D2.1.1_YR1_ATBD-MERIS_v1.1 |      |            |
|   |  | Issue | 1.1                                 | Date | 11/11/2016 |
|   |  |       |                                     |      | Page       |

- Asrar, G., editor, Theory and Applications of optical Remote Sensing, pages 336–428. Wiley and Sons, New York.
- Martín, M.P., Gómez, I., & Chuvieco, E. (2005). Performance of a burned-area index (BAIM) for mapping Mediterranean burned scars from MODIS data. In J. Riva, F. Pérez-Cabello, & E. Chuvieco (Eds.), Proceedings of the 5th International Workshop on Remote Sensing and GIS applications to Forest Fire Management: Fire Effects Assessment (pp. 193-198). Paris: Universidad de Zaragoza, GOCF-GOLD, EARSeL.
- Mekler, Y. and Kaufman, Y. J. (1982) Contrast reduction by atmosphere and retrieval of nonuniform surface reflectance. Applied Optics, 21:310–316.
- Oliva, P., Martín, P., & Chuvieco, E. (2011). Burned area mapping with MERIS post-fire image. International Journal of Remote Sensing, 32, 4175-4201.
- Padilla, M., V. Stehman S., Hantson S., Oliva P., Alonso-Canas I., Bradley A., Tansey K., Mota B., Pereira JM, & E., C. (2015). Comparing the Accuracy of Global Burned Area Products using Stratified Random Sampling. Remote Sensing of Environment, 120, 114-121.
- Pereira, J.M.C. (1999). A Comparative Evaluation of NOAA/AVHRR Vegetation Indexes for Burned Surface Detection and Mapping. IEEE Transactions on Geoscience and Remote Sensing, 37, 217-226
- Pereira, J.M., Mota, B., Oom, D., Calado, T., Alonso, I., Oliva, P., González-Alonso, F., (2014) D3.6.2 - Algorithm Theoretical Basis Document – Volume II – BA Algorithm Development, version 2.2. [http://www.esa-fire-cci.org/webfm\\_send/850](http://www.esa-fire-cci.org/webfm_send/850).
- Ph1\_PVASRv2.0 (2012) CCI-LC PVASR Phase I. Land Cover Climate Change Initiative Product Validation Algorithm Selection Report – only available on request
- Ph2\_ATBDv1.1 (2016) CCI-LC ATBD Phase II. Land Cover Climate Change Initiative - Algorithm Theoretical Basis Document – only available on request.
- Pinty, B., & Verstraete, M.M. (1992). GEMI: a non-linear index to monitor global vegetation from satellites. Vegetatio, 101, 15-20.
- Preusker et al., (2008) MERIS Global Land Surface Albedo MAPS ATBD Cloud detection, issue: 4, rev.:0.
- Pu, R.L., Li, Z.Q., Gong, P., Csiszar, I., Fraser, R., Hao, W.-M., Kondragunta, S., & Weng, F. (2007). Development and analysis of a 12-year daily 1-km forest fire North America from NOAA/AVHRR data. Remote Sensing of Environment, 108, 198-208.
- Roy, D.P., Giglio, L., Kendall, J.D., & Justice, C.O. (1999). Multi-temporal active-fire based burn scar detection algorithm. International Journal of Remote Sensing, 20, 1031-1038.
- Santer, R. and Aznay, O., (2008). Direct to direct O2 transmittances: Determine the surface pressure. LISE, Internal Technical Note.
- Santer, R and Ramon, D., (2011) MERIS ATBD - Aerosol remote sensing over land,

|   |  |  |       |                                     |      |            |
|---|--|--|-------|-------------------------------------|------|------------|
|  | <b>Fire_cci</b><br><b>Algorithm Theoretical Basis</b><br><b>Document – MERIS</b> |  | Ref.: | Fire_cci_D2.1.1_YR1_ATBD-MERIS_v1.1 |      |            |
|   |  |  | Issue | 1.1                                 | Date | 11/11/2016 |
|   |  |  |       |                                     | Page | 48         |

ATBD2.15, v4

- Schoenermark et al. (2004) Reflection properties of Vegetation and soil - with a BRDF database, publisher Wissenschaft & Technik Verlag.
- Stamnes, K., Tsay, S. C., Wiscombe, W., and Jayaweera K. (2007) Numerically stable algorithm for discrete-ordinate method radiative transfer in multiple scattering and emitting layered media, Appl. Optics, 27, 2502-2510
- SYN\_DPMv2.3 (2010) SYN Detailed Processing Model version 2.3 – only available on request.
- Tansey, K. Bradley, A. and Padilla, M. (2014): D3.6.3 - Algorithm Theoretical Basis Document – Volume III – BA Merging. ESA Fire\_cci project, available at available at <http://www.esa-fire-cci.org>.
- Vermote, E. F., El-Saleous, N., Justice, C. O., Kaufman, Y. J., Privette, J. L., Remer, L., Roger, J. C., and Tanré, D. (1997a) Atmospheric correction of visible to middle infrared EOS-MODIS data over land surface: Background, operational algorithm and validation, Journal of Geophysical Research, 102:17131–17141.
- Vermote, E. F., Tanré, D., Deuzé, J. L., Herman, M., and Morcrette, J. J. (1997) Second Simulation of the Satellite Signal in the Solar Spectrum, 6S: An overview, IEEE Transactions on Geoscience and Remote Sensing, 35:675–686.
- Zagolski, F. and Goryl, P. (2011), ENVISAT 1 – Ground Segment – MERIS - Specification of the scientific contents of the MERIS L1b & L2 Auxiliary Data Products, PO-RS-PAR-GS-0002 issue 3, revision C.



## Annex 1: Acronyms and abbreviations

|         |  |
|---------|--|
| AD      | Applicable Document  |
| AMF     | Air Mass Factor  |
| AMORGOS | Accurate MERIS Ortho Rectified Geo-location Operational Software |
| AOD     | Aerosol Optical Depth  |
| ATBD    | Algorithm Theoretical Basis Document                             |
| AVHRR   | Advanced Very High Resolution Radiometer                         |
| BA      | Burned Area  |
| BDRF    | Bidirectional Reflectance Distribution Function                  |
| CBH     | Cloud Base Height  |
| CCD     | Charge-couple device   |
| CCI     | Climate Change Initiative  |
| CCI-LC  | Land Cover CCI project   |
| CDF     | Cumulative Distribution Function                                 |
| CTP     | Cloud Top Height   |
| CWV     | Water Vapour Column Content                                      |
| DOM     | Dark Object Method   |
| ENVISAT | ENVironmental SATellite  |
| EO      | Earth Observation  |
| ECV     | Essential Climate Variables                                      |
| ELEV    | Elevation  |
| ESA     | European Space Agency  |
| ETM+    | Enhanced Thematic Mapper Plus                                    |
| FIRMS   | Fire Information for Resource Management System                  |
| FR      | Full Resolution  |
| FRS     | Full Resolution Swath  |
| FSG     | Full Resolution Geo-corrected                                    |
| FTP     | File Transfer Protocol   |
| GCOS    | Global Climate Observing System                                  |
| GEMI    | Global Environmental Monitoring Index                            |
| HS      | Hotspot  |
| HSV     | Hue Saturation Value   |
| IPCC    | Intergovernmental Panel on Climate Change                        |
| LARS    | Land Aerosol Remote Sensing                                      |
| LC_cci  | Land Cover CCI   |
| MERIS   | Medium Resolution Imaging Spectrometer                           |
| MIR     | Medium Infra-Red   |
| MDSI    | MERIS differential snow index                                    |
| MODIS   | Moderate Resolution Imaging Spectroradiometer                    |
| MOMO    | Matrix-Operator-Model  |



|        |   |
|--------|---|
| n.a.   | Not applicable                                    |
| NDII   | Normalized difference ice index                   |
| NDVI   | Normalized difference vegetation index            |
| NDSI   | Normalized difference snow index                  |
| NIR    | Near InfraRed                                     |
| NN     | Neuronal Net                                      |
| OZO    | Ozone Column Content                              |
| PAF    | Potential Active Fire                             |
| PVASAR | Product Validation and Algorithm Selection Report |
| QA     | Quality assessment                                |
| RAA    | Relative Azimuth Angle                            |
| RGB    | Red-Green-Blue colour model                       |
| RMS    | Root mean square                                  |
| RR     | Reduce resolution                                 |
| RRG    | Reduce Resolution Geocorrected                    |
| SAA    | Sun Azimuth Angle                                 |
| SDR    | Surface Directional Reflectance                   |
| SPOT   | Satellite Pour l'Observation de la Terre          |
| SR     | Surface reflectance                               |
| SRTM   | Shuttle Radar Topography Mission                  |
| SWBD   | SRTM Water Body Data                              |
| SWIR   | ShortWave InfraRed                                |
| SZA    | Sun Zenith Angle                                  |
| TIR    | Thermal Infra-red                                 |
| TM     | Thematic Mapper                                   |
| TOA    | Top of Atmosphere                                 |
| VAA    | View Azimuth Angle                                |
| VGT    | Vegetation  |
| VZA    | View Zenith Angle                                 |